AD-A173 310 EXPERIMENTAL STUDY OF TURBULENCE PRODUCTION MECHANISMS IN BOUNDARY LAYER..(U) MICHIGAN STATE UNIV EAST LANSING TURBULENCE STRUCTURE LAB R E FALCO MAY 85 TSL-85-1 1/1

UNCLASSIFIED AFOSR-TR-86-0960 F49620-82-K-0003 F/G 20/4 NL

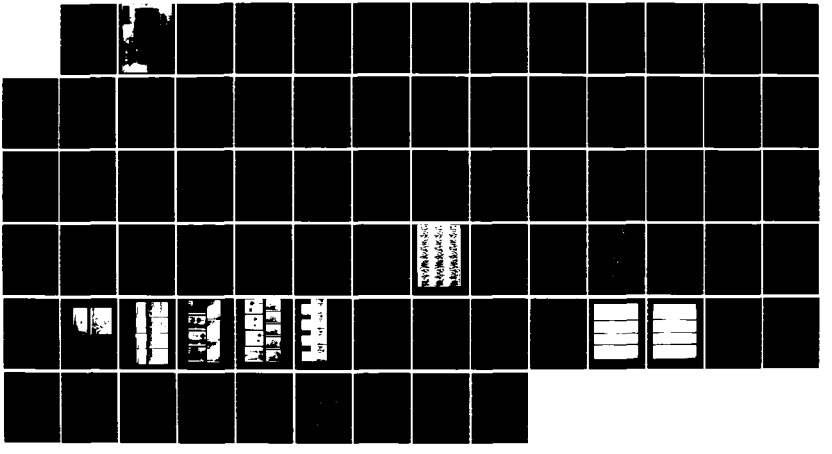

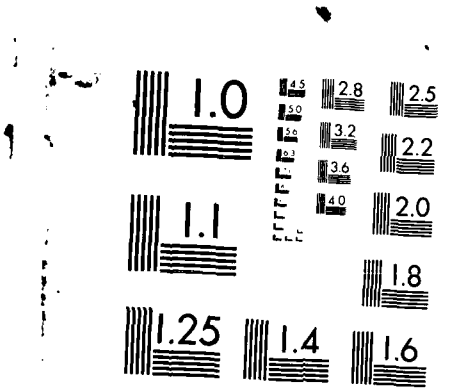

EXPERIMENTAL STUDY OF TURBULENCE PRODUCTION MECHANISMS IN BOUNDARY LAYER FLOWS

by

R. E. Falco

Principal Investigator

Final Report

Prepared from work done under
Air Force Office of Scientific Research
Contract F49620-82-K-0003

Report TSL 85-1

TURBULENT STRUCTURE LABORATORY
DEPARTMENT OF MECHANICAL ENGINEERING
MICHIGAN STATE UNIVERSITY
EAST LANSING, MI 48824

EXPERIMENTAL STUDY OF TURBULENCE PRODUCTION MECHANISMS IN BOUNDARY LAYER FLOWS

by

R. E. Falco

Principal Investigator

Final Report

Prepared from work done under
Air Force Office of Scientific Research
Contract F49620-82-K-0003

Report TSL 85-1

Turbulence Structure Laboratory
Department of Mechanical Engineering
Michigan State University
East Lansing, MI 48824

May, 1985

UNCLASSIFIED

AD-A161 310

REPORT DOCUMENTATION PAGE

1a. REPORT SECURITY CLASSIFICATION: Unclassified	1b. RESTRICTIVE MARKINGS
2a. SECURITY CLASSIFICATION AUTHORITY	3. DISTRIBUTION / AVAILABILITY OF REPORT: Unlimited
2b. DECLASSIFICATION / DOWNGRADING SCHEDULE	
4. PERFORMING ORGANIZATION REPORT NUMBER(S)	5. MONITORING ORGANIZATION REPORT NUMBER(S): AFOSR-TR- 86-0960
6a. NAME OF PERFORMING ORGANIZATION: Michigan State University	6b. OFFICE SYMBOL (If applicable):
6c. ADDRESS (City, State, and ZIP Code): East Lansing, MI 48824	7a. NAME OF MONITORING ORGANIZATION: AFOSR
	7b. ADDRESS (City, State, and ZIP Code): AFOSR/NA, Bolling Air Force Base, Washington, DC
8a. NAME OF FUNDING / SPONSORING ORGANIZATION	8b. OFFICE SYMBOL (If applicable): NA
8c. ADDRESS (City, State, and ZIP Code): Same as 7b	9. PROCUREMENT INSTRUMENT IDENTIFICATION NUMBER: ~~AFOSR Contract No.~~ F49620-82-K-0003
	10. SOURCE OF FUNDING NUMBERS: PROGRAM ELEMENT NO. 61102F; PROJECT NO. 2307; TASK NO. A2; WORK UNIT ACCESSION NO.

11. TITLE (Include Security Classification)
Experimental Study of Turbulence Production Mechanisms in Boundary Layer Flows

12. PERSONAL AUTHOR(S)
R. E. Falco

13a. TYPE OF REPORT	13b. TIME COVERED	14. DATE OF REPORT (Year, Month, Day)	15. PAGE COUNT
FINAL	FROM 10/1/82 TO 9/30/84	1985 May	72

16. SUPPLEMENTARY NOTATION

17. COSATI CODES		
FIELD	GROUP	SUB-GROUP

18. SUBJECT TERMS (Continue on reverse if necessary and identify by block number)
Turbulence, production, vortices, boundary layers, bursting, flow visualization, vorticity, hot-wire anemometry, vortex-in-cell

19. ABSTRACT (Continue on reverse if necessary and identify by block number)

Studies of the structure of turbulence near a wall have shown that the production process has many manifestations. A unifying conceptual framework within which the experimental observations can be comprehended does not exist, but would be of great value to engineers seeking to manipulate drag and heat transfer characteristics. Detailed experiments, involving visual information in two mutually orthogonal planes, and simultaneous multiple hot-wire anemometry, along with both experimental and numerical simulations have been performed in an attempt to determine the underlying conceptual framework. Results indicate that the wide variety of evolutions observed during the turbulence production process near a wall are all manifestations of the evolution of vortex ring-like eddies with the wall and the wall layer. Additional important evolutions are the result of the interaction of two of these vortex ring/wall
(see other side)

20. DISTRIBUTION / AVAILABILITY OF ABSTRACT	21. ABSTRACT SECURITY CLASSIFICATION
☐ UNCLASSIFIED/UNLIMITED ☐ SAME AS RPT ☐ DTIC USERS	
22a. NAME OF RESPONSIBLE INDIVIDUAL: DR JAMES MCMICHAEL	22b. TELEPHONE (Include Area Code): 202-767-4935 / 22c. OFFICE SYMBOL: NA

19. ABSTRACT (Continued)

interactions occurring with small spatial and temporal differences. By separating out the influence of a number of different mechanisms we have arrived at an ordered picture of the process of turbulence production near a wall in a turbulent boundary layer. Boundary layer interactions have been divided into four classes; ranging from weak interactions creating little or no turbulence, to ones producing strong turbulence. These four classes have been simulated by experimental studies of vortex ring/moving wall interactions, and -- within the constraints of two-dimensions -- qualitatively by simple numerical vortex-in-cell simulations. Two conditions play a dominant role determining which class of evolution is observed. One is the instantaneous local thickness of the viscous sublayer. The other is the flow field of the large scale motions, which influence both the relative convective velocity and the angle of approach of the ring-like eddies which initiate new turbulence near a wall. Both the experimental simulations of the eddy-wall interaction and the numerical calculations have shown that there are well defined critical combinations of relative convection velocity, angle of approach and ring to wall layer thickness, which result in the strong interactions.

ACKNOWLEGDMENTS

This research was sponsored under Contract F49620-82-K-0003, the Air Force Office of Scientific Research, United States Air Force.

Air Force Technical Project Manager for this program is Major Michael Francis, AFOSR.

The numerical simulations presented were performed by Prof. R. W. Bartholomew. His assistance is greatly appreciated.

A1

ABSTRACT

Studies of the structure of turbulence near a wall have shown that the production process has many manifestations. A unifying conceptual framework within which the experimental observations can be comprehended does not exist, but would be of great value to engineers seeking to manipulate drag and heat transfer characteristics. Detailed experiments, involving visual information in two mutually orthogonal planes, and simultaneous multiple hot-wire anemometry, along with both experimental and numerical simulations have been performed in an attempt to determine the underlying conceptual framework. Results indicate that the wide variety of evolutions observed during the turbulence production process near a wall are all manifestations of the evolution of vortex ring like eddies with the wall and the wall layer. Additional important evolutions are the result of the interaction of two of these vortex ring/wall interactions occurring with small spatial and temporal differences. By separating out the influence of a number of different mechanisms we have arrived at an ordered picture of the process of turbulence production near a wall in a turbulent boundary layer. Boundary layer interactions have been divided into four classes, ranging from weak interactions creating little or no turbulence, to ones producing strong turbulence. These four classes have been simulated by experimental studies of vortex ring/moving wall interactions,

and--within the constraints of two-dimensions--qualitatively by simple numerical vortex-in-cell simulations. Two conditions play an dominant role determining which class of evolution is observed. One is the instantaneous local thickness of the viscous sublayer. The other is the flow field of the large scale motions, which influence both the relative convective velocity and the angle of approach of the ring-like eddies which initiate new turbulence near a wall. Both the experimental simulations of the eddy/wall interaction and the numerical calculations have shown that there are well defined critical combinations of relative convection velocity, angle of approach and ring to wall layer thickness, which result in the strong interactions.

TABLE OF CONTENTS

1.1 OVERVIEW OF THE RESEARCH PRESENTED

Many features of the turbulence production process have been clarified in this latest work. The most important result is that a single flow module can be used to describe the different evolutions observed by us and many other investigators. A vortex ring-like eddy interacting with the sublayer shear in the neighborhood of the wall is at the heart of the production process. In spite of the unique originating flow module, the strength of the new turbulence produced, and the new forms of fluid motion resulting from the interaction, critically depend on the local thickness of the wall layer, the relative vorticity of the initiating eddy and the vorticity distribution instantaneously existing in the wall region, and the angle of flight of the initiating eddy (which depends in large measure on the large scale motions). These results contain both good and bad news. The bad news is that it was, and will continue to be, very difficult to piece together and quantify the complete picture of physical processes by experimentation in the boundary layer alone--simulations both experimental and numerical will play important roles. The good news is that a preliminary overall model with substantial experimental support has now been formulated. An important outcome of this new understanding is that the above mentioned sensitivity enables us to appreciably effect the turbulence production process with a correctly applied small change in

wall conditions, or by modifying the large eddies using outer flow manipulators. An example in the wall region is the drag reducing effect of riblets, which we can now argue occurs simply as a result of the riblets effectively thickening the viscous sublayer. In the outer region, thin plates or airfoils which modify the large scale flow fields that govern the orientation of the initiating eddies, will also influence the production mechanism and hence the drag produced.

1.2 BACKGROUND

It has proven to be very difficult to determine the physical processes that initiate the bursting process (the name given to the overall event which results in the production of new turbulence near a wall), because we must detect the event to study it. We will not attempt to review the current state of affairs. The reader is referred to Ref. 1 and 15 for reviews and further references.

When the current work was initially undertaken in September 1981, we had discovered that the interaction of outer region motions left a footprint in the wall region that was associated with most of the Reynolds stress produced in the wall region (see Ref. 1). Examination of hot-wire measurements taken simultaneously with the flow visualization movies, indicated that these 'pockets' were the result of outer region eddies interacting with the wall. By placing a laser sheet above the wall and through separately marking the outer region flow with an upstream slit, we were able to observe, although not clearly, evidence of vortex ring-like eddies interacting with the wall when a pocket formed. Fig. 1 and 2 show the arrangement of the slits, laser, flood light, mirrors, probes, camera and clock used to obtain the data. With this evidence as background, we proceeded to design and perform experiments which would verify or argue against this evidence. Our goal

was to obtain a statistically significant visual sample of the prevalent mechanisms, and to obtain ensembles of the magnitude of the turbulence produced by the interactions.

We somewhat artificially divided the mechanisms into; 1) the formation of the pocket footprints in the wall layer, 2) the evolution of the pockets, and the resulting vortices, 3) interaction of the ejecting wall layer fluid with the outer flow field.

An important finding of this study is our understanding of where different structural features of the bursting process, which have been observed by different investigators, fit into the overall picture.

1.3 RESULTS OF WALL LAYER FLOW FEATURES

The section is divided into 4 parts. We start with a discussion of the footprint of the forcing function, which leaves pockets and streaks in the wall region. Second, we review our new knowledge of the eddies which initiate the production process, which are shown to be the Typical eddies also found in the outer part of the boundary layer (Falco 1977). Then we describe the coherent motions which result from the interaction of the vortex ring-like Typical eddies with the

viscous sublayer and the wall. Next, we discuss the dynamics of wall layer fluid that gets out of the wall region; this has been observed to breakdown and form new production initiating Typical Eddies. We then review experiments that further describe the Typical eddies. Followed by experiments that quantify the large scale motions, and finally attempt to tie all the results together.

All of our boundary layer results have come from experiments which used flow visualization and hot-wire anemometry simultaneously. The interpretations, in each case, have both the picture and the signal to support them. Some of the interpretations are, however, based on Lagrangian visual information, which for the type of experiments we are currently doing can only be qualitative. The vortex ring/wall shear layer experiments can supply only visual information.

1.3.1 STREAKS AND POCKETS

We have only recently understood why flow visualization techniques appeared to give different pictures. It is now clear Ref 3, that if very little marker is put into the sublayer of the flow (see Ref. 4-7) we can only see the regions where the marker concentration is above the visual threshold. Under these circumstances, the bursting process reveals itself

as an oscillation and lifting of these streaks. If we put in enough marker to fill about 1/2 of the sublayer or more, we can see the flow in between the streaks. These experimental conditions reveal that the process is characterized by the clearing of a local region of fluid. This 'scooping out' of wall layer fluid occurs both in between the existing streaks, and on them, and leaves a 'pocket' of unmarked fluid. When it occurs on an existing streak, the streak appears to oscillate and lift up.

These results are described more fully in Ref 8. Both frequency and spatial data has been measured for pockets, and spatial data has been measured for streaks. Ref. 3, 4, 5 and 9 (among others) have shown that the streak spacing scales on wall layer variables. Ref. 10, 11, 12 and 13 have shown that the pockets do not scale on wall variables or the recently suggested mixed variables of Ref. 14.

The pocket evolution has been divided into five stages, and signals in each stage ensemble averaged (see Ref 1). Fig. 3 shows a photo of a pocket and Fig. 4 shows the five stages of evolution pockets can evolve through. Stages I and II indicated that outer layer fluid produced high Reynolds stress in a motion called a sweep. Stages III and IV were initially thought to be a consequence of self induction of the redistributed wall layer vorticity. They showed that the

sweeps evolved into ejections, which also produced high Reynolds stresses. Stage five was thought to be due to shear layer breakdown. Many authors agreed in general with this mechanism of the breakdown (Blackwelder, Landahl Etc) of the lifted wall layer fluid. However, we now understand the breakdown to be intimately tied to the initiating eddy. It is not a shear layer breakdown as we shall describe later. We have since learned that all pockets don't go through the same set of stages. It was necessary to have simultaneous laser sheet visual data of the outer flow above the pockets, and a flood light illuminated wall region to show the pockets for us to understand this; a capability not available in 1979, when the data of Ref. 13 was obtained.

1.3.2 EDDIES WHICH INITIATE THE PRODUCTION PROCESS

Our initial experiments were set up to determine the form of event/eddy that initiated the production process. These experiments showed that pockets were initiated by vortex ring-like eddies of a particular orientation (see Fig. 5a). Our earlier data had shown, as indicated in the 1980 proposal, that rings of both orientations indicated in Fig. 5 were responsible for the formation of pockets. Our new higher resolution data has indicated that these events are not independent. We have observed that the passage of eddies of

orientation in Fig. 5a often result in a flow rearrangement that appears, in a limited field of view to be a vortex ring of the orientation in Fig. 5b. This was explained in Ref. 15, and is summarized in Fig. 6. In this case we do not have a ring upstream, but instead the lower part of a ring and the head of a hairpin just upstream, which had been generated by the ring just downstream of it. Fig. 7 shows the ensemble averaged u, v, and uv data from the passage of the predominant initiating eddy. The measurements confirm the importance of the event, and show the similarity of the flow in the ring at $y+ = 24$, and that in the pocket at $y+ = 16$.

A second important conclusion is that these eddies not only initiate the turbulence production process, but are essentially involved in the various observed evolutions of that process.

1.3.3 COHERENT MOTIONS RESULTING FROM THE INTERACTIONS

Experiments similar in kind to those used to determine the eddies which initiate the turbulence production process, were performed to examine the later stages of it, which result in various types of ejections, mixing and breakdown. The essential difference in experimental technique from that used in the previous section is that the laser sheet is now placed

so that the second (downstream) slit is in the upstream portion of the frame, and the probe is placed further downstream of the second slit. It was necessary to do this because the laser sheet did not have the intensity to spread over the evolutionary distance, and furthermore, with the probe placed so as to quantify the early stages, it seriously influenced the later evolution which had to occur over the probe support. Along with the differing evolution of the pockets, because we had a four wire cross-stream vorticity probe in the flow, we discovered that, although we usually obtained high instantaneous Reynolds stress signatures due to the sweep caused by the ring that initiates the pocket, we often did not get either high uv or high vorticity signatures characteristic of an ejection when the pockets did not evolve. Furthermore, we found that incident rings that appeared to be similar in scale and coherence, didn't always result in a pocket completely forming, or result in the strong mixing sometimes observed. After a period of confusion lasting about 18 months, I finally began to make sense of the situation. Fig. 8 shows the breakdown necessary to unravel the puzzle. It is important to point out that the unraveling of this situation involved two other pieces of research; the vortex ring/wall studies and the numerical simulations described later.

Visually, their are four types of evolutions. Fig. 8 shows that all of the stages of the pocket evolution do occur,

but that they depend upon whether the incident vortex ring-like Typical eddy/wall interaction results in the breakup of the ring or not. This is an important improvement in our understanding. It appears that it is not the self-induced evolution of the wall layer that governs the evolution from a sweep into an ejection. Proponents of the hypothesis that shear layer instabilities of the mixing layer type can generate hairpins, have argued that self-induction of the hairpins has led to the outward movement. Instead, we have found that the transformation from sweep to ejection is a continuing result of the induction effects of an incident vortex ring-like Typical eddy. With the experimental information that we have so far gathered in the turbulent boundary layer, we can only report on the outcomes of the interaction in the laser sheet side view, and simultaneous flood illuminated plan views. Four outcomes have been observed as the Typical eddy approaches the wall:

a) The incident eddy opens a pocket (Stage I, possibly Stage II), then leaves the interaction essentially 'in tact'. In this case no wall layer fluid gets into the ring-like eddy, and the wall layer is only weakly rearranged. No mixing of eddy and wall layer fluid occurs, and the wall layer relaxes back to its undisturbed state. Thus, the pocket never develops, and we have essentially no new turbulence produced. This interaction will produce little drag.

b) The incident ring-like eddy opens a pocket, which we see evolving further, all the way through Stage IV. The laser sheet side view shows us that the ring like-eddy induces this fluid up away from the wall, but that it doesn't get ingested into the eddy. The eddy goes on to survive the interaction 'in tact', as in Type 1 interactions. Thus, there is no mixing of outer layer ring fluid with the wall layer fluid, consistant with Type 1 interactions. However, the difference is that the ring has redistributed wall layer fluid into a 'hairpin vortex' and mutual induction of this hairpin and the lower part of the vortex ring has caused this vortex to move away from the wall up into the buffer and perhaps the log region. It is the ring which is responsible for this outward movement, not self-induction of the hairpin. Observations show that the ring which is traveling faster than the lifted hairpin, eventually moves downstream of it, and the outward movement of the hairpin ceases. At times it even moves back towards the wall.

Some very recent experiments have revealed that a pair of hairpins can be formed by the Type 2 interaction.

Both Type 1 and Type 2 interactions, are ones in which the initiating vortex ring-like eddy does not break-up. We call these interactions stable vortex/wall interactions.

c) The incident ring-like eddy opens up a pocket which we see

evolve through all Five stages. In this case, termed Type 3, the ring induces wall layer fluid upward from the downstream end of the pocket. This fluid briefly assumes a 'hairpin' vortex shape, then is rapidly ingested into the ring itself. The ring changes direction and begins to move away from the wall, but the ingested fluid, causes it to become unstable, and violent breakup into fine scales results, with ensuing strong mixing. This breakup occurs partially in the wall region and partially in the outer region, thus contributing both to the drag and to the outer layer transport of new turbulence.

d) The incident ring-like eddy opens up a pocket which also evolves through all five stages. This case, termed Type 4, is characterized by the fact that the ring ingests fluid into it and breaks up before the ring can change direction and begin movement away from the wall. The fluid induced away from the wall (the ejection) hardly has time to form into a hairpin, and furthermore, it does not move out of the buffer region before being ingested. In this case the mixing is confined to the wall region and the highest drag results.

Type 3 and Type 4 events involve the breakup of the ring-like Typical eddy and of the ejected fluid, and are termed 'unstable' Typical eddy/wall interactions.

Before discussing the reasons we have found behind these

differences, we need to point out that the hot-wire signals resulting from the four Types of interaction, for a probe at a fixed height, will be very different. The ensemble averaged signals for the five stages in Fig. 4 show the details of these differences. It is also true that for a given type of event, the signals recorded by a hot-wire probe will be very different depending upon the position of the wire above the wall as shown in Fig. 9.

1.3.4 LATER DEVELOPMENT OF LIFTED HAIRPINS-BASIS OF A PRODUCTION CYCLE

With the experimental apparatus set up so that we can observe the evolution of marker from the second slit for about three boundary layer thicknesses, we had the opportunity to occasionally witness the evolution of an ejection that got beyond the wall region. The very interesting outcome of the limited number we captured in the high speed movies (see Ref. 15) was that the upper portion of these hairpins were observed to break down and form vortex rings. This process was reminiscent of the breakdown of aircraft trailing vortices. An important difference is that it is occurring in an ambient of high fluctuating vorticity, and high shear, and thus it is reasonable to expect the process to be accelerated.

This evolution of the ejection into a new vortex ring-like

Typical Eddy brings us full circle, and establishes the basis for further production of new turbulence. This conclusion is in agreement with the results of Ref. 16, although we have added significant detail to the picture. It is important to emphasize that we have witnessed the event less than ten times, which is in part due to the low light levels obtained when the laser sheet is spread so far (this should be corrected when the Copper Vapor laser finally comes), and possibly because the event is not the crucial Typical eddy creation mechanism. More studies are needed to determine the answer.

1.4 VORTEX RING/WALL SHEAR LAYER SIMULATION EXPERIMENTS

In the light of our findings in section 1.3.3, a key task of our investigation has been to design experiments which would help us to determine the reasons behind the existence of the four distinct types of interactions observed. By modeling the ring-like Typical eddy with an artificially generated vortex ring, and simulating the viscous sublayer with a Stokes layer, generated by impulsively starting a moving belt, we could vary the important parameters of the interaction, and determine their relative importance.

Fig. 10 shows how the use of the Galilean transformation brings the two experiments into coincidence. Figures 11, 12,

13 show how well the model qualitatively simulates the Types 1, 3 and 4 interactions. Fig. 11 shows both the plan and side views of a turbulent boundary layer, and the vortex ring /wall shear layer simulation. The sequences proceed from right to left. A vortex ring-like Typical eddy in the boundary layer interacts with the wall, creates a pocket and then leaves the wall region in tact--i. e. undergoes a Type 1 interaction. In the lower half of the figure we can also see the vortex ring moving towards the wall, then change direction and move away 'in tact'.

Fig. 12 shows plan and laser sheet side views of both the turbulent boundary layer, and the vortex ring/wall simulations for the Type 3 interaction, where the ring breaksup after leaving the wall region. In both cases we can see the pocket forming, then the coherent ring loses its coherence in the lower lobe as it moves away from the wall. The resulting boundary layer photo could easily be mistaken for a hairpin vortex that might be thought to have created the pocket--a suggestion put forth by Smith (private communication).

Fig. 13 shows plan and laser sheet side views of a Typical eddy in a turbulent boundary layer undergoing a type 4 interaction. The Reynolds stresses and vorticity resulting from this interaction are also shown. On the left side of the figure the vortex ring/wall shear layer simulation is

presented. We can see the excellent visual comparison, and we can also see that the lower lobe of the ring-like eddy undergoes strong vorticity amplification; compare with the ensemble averages of his event in Fig. 7.

The important parameters in the modeling are:

a) the magnitude of circulation of the ring with respect to that of the wall,
b) the diameter of the ring with respect to the thickness of the wall layer,
c) the angle of incidence of the ring with the wall.

Experiments were performed for rings incident at three angles covering the range observed in the boundary layer. An essential experimental difficulty in these simulations, was the measurement of the thickness of the layer developed on the moving belt. This was solved using the Photochromic technique in a second tank with kerosene as the working fluid. Fig. 14 shows a comparison of an experimentally obtained profile with the exact solution of the boundary layer on an impulsively started moving belt. Making use of data of this type, we were able to produce parameter maps showing the conditions under which the ring/wall shear layer interactions remained stable (i. e. were similar to Type 1 and Type 2 found in the turbulent boundary layer), and conditions under which the interactions were unstable (Types 3 and 4 found in the boundary layer).

Fig. 15 shows the results found for 15 degree rings,

Fig. 13 shows the effects of changing the incident angle. Because these experiments are well defined and reproducible, we can say with confidence that for a fixed geometry, it is the ratios of the the parameters delta/D and Ur/Uw that govern the stability of interactions of this type. For the 15 degree ring we can see that in the range of convection velocities that are found in the boundary layer, the relative thickness of the sublayer to that of the incident ring is an extremely important factor determining the strength of the interaction that will occur. Although the data points represent the average position of the stability boundary, it is relatively sharp, so that small changes in either the thickness ratio or the convection velocity of the incident eddy can completely change the picture.

Fig. 16 shows that the effect of changes in the angle of incidence of the ring can markedly change the stability of the interaction--all other factors kept constant.

From these results it is clear that the boundary layer has built into its variability the possibility of very little or a lot of drag with each interaction.

The physical process behind the different interactions turn out to be very simple. Lets take the case were the strength of the ring and that of the wall layer is fixed. What

will determine whether the interaction is strong (Types 3, 4) or weak (Types 1, 2)? The competing mechanisms are the overall rotation about the center of gravity of the ring caused by the fact that the lower part of the ring is in a higher velocity region than the upper part (i. e. in the wall shear layer), and the fact that the inviscid impermeability condition acts to decelerate the part of the ring closest to the wall. The first mechanism acts to change the rings direction making it move away from the wall, while the second tends to turn it into the wall. The impermeability condition also acts to stretch the ring. This amplifies its vorticity. Now the shear in a thick wall layer begins to act upon the incoming ring before the ring comes close enough to the wall for the impermeability condition to become important. Thus, the ring can be turned away from the wall before ingesting wall layer fluid, and therefore not breakup. On the other hand, a thin wall layer does not begin to effect the ring before the impermeability condition takes effect. If this effect dominates, the ring will induce wall layer fluid into it and breakup.

It is easy, in the light of these experiments to see why we observed such a large variability in the intensity and form of the interactions of vortex ring-like eddies with the wall region in a turbulent boundary layer. For example, at any instant for an eddy of given strength, depending on the local instantaneous thickness of the viscous sublayer, any

interaction ranging from Type 1 to Type 4 could take place. If the instantaneous sublayer thickness was a little greater, a condition that would exist if either the last strong interaction had occurred some time ago, or, if a Type 1 interaction had just recently occurred, very little drag or momentum transfer would result from the interaction (another Type 1 would likely occur).

1.5 NUMERICAL SIMULATIONS

Since vortex stretching definitely occurs when the ring comes under the influence of the impermeability condition, an important fact to determine is whether the overall effect, i. e. a stable--weak interaction vs. an unstable--strong interaction is governed by these mechanisms in their essentially two-dimensional form or whether three-dimensional effects are important at the go -- no-go level.

Work on this project has been jointly done with Professor R. W. Bartholomew, who has performed all of the computational aspects on an LSI 11/23 microcomputer. Briefly, a vortex-in-cell technique has been used to model the ring/impulsively started moving wall experiments. The overall arrangement is shown in Fig. 17, where the subregion of the computational domain which defines Fig. 18, 19, is also

indicated. The input to the calculations is the vorticity distribution in the wall layer, which is an exact solution of the Navier Stokes Equations, and the speed and angle of the ring. There are no adjustable constants. Some results of the calculation in this subregion for thick and thin wall layer experiments, with all other aspects identical are shown in Fig. 18, Fig. 19 and Fig. 20. Fig. 18 shows the results of a two-dimensional simulation of the experiment shown in Fig. 13. The calculations were stopped at approximately Fig. 13b. Fig. 19 shows calculations corresponding to conditions of Fig. 11. The results of these calculations have shown that the stability/instability of the ring/wall shear layer interactions is essentially governed by two-dimensional mechanisms. This is extremely important when we consider engineering capabilities available to modify the drag.

Fig. 20 indicates the quantitative stability map comparisons. These show that the detailed comparisons are not very good. However, this was expected, because we have not included three-dimensional mechanisms, which should be important in terms of amplifying the ingestion--through vortex stretching--and in accelerating the breakdown and mixing process. We do not have the means, under the current contract, to access the computing capability needed to extend the calculations to three dimensions.

1.6 LARGE SCALE MOTIONS AND THEIR EFFECT ON THE PRODUCTION PROCESS

An important outcome of the vortex ring/wall shear layer experiments is that small changes in the angle of the ring have a large effect on the stability of the interaction (see in Fig. 16). In particular, there is a trend towards greater stability as the angle of the ring decreases. Since the large scale motions of the outer region set up flow fields in the wall region which have a large effect on the motion of the vortex ring-like eddies (see Ref. 2) both towards and away from the wall, an understanding of the flow fields of the large scale motions is a necessary part of our understanding of the turbulence production process. We have used our simultaneous hot-wire anemometry and flow visualization capability to obtain ensemble averages of the flow field in the large eddies at four Reynolds numbers RTHETA = 730, 1356, 2745 and 3116. In Fig. 21 and 22 the solid lines show the Reynolds stress distribution, the vorticity distribution, as well as the streamwise and normal velocity signatures, and some velocity derivative signatures at RTHETA = 730 and 2745. Other derivatives and transport terms (not shown) were also investigated. The results indicate that the large scale motions have a well defined outward motion within them and that a well defined wallward motion is established both upstream and downstream of them at y/delta approximately .8. The ensemble averaged strength of these motions indicates that if they persist, even

at a diminished magnitude, further in the boundary layer, they could have a governing effect on the path of the Typical eddies; contributing both to their motion towards the wall (creating drag) as well as away from it. It is already known that devices put into the outer region (called LEBU's, Manipulators, TAPPM's, etc.), can significantly influence the drag on the wall, although the reason behind their influence is not yet understood.

Three facts need to be established. First, how does the relative strength of the large scale motions change as the Reynolds number increases? Second, how does the strength of the large scale motions compare with the strength of the Typical eddies own self-induced motion? Finally, as the Typical eddies vary with Reynolds number, does the influence of the large scale motions on determining the direction of the Typical eddy interaction with the wall increase or decrease?

The first question has been addressed over the range of Reynolds numbers studied. As indicated by comparing Fig. 21 and Fig. 22 the results non-dimensionalized by the freestream velocity and momentum thickness adequately remove the Reynolds number dependence. To answer the second and third questions, we needed to study the Typical eddies.

1.7 TYPICAL EDDIES; THEIR STRENGTH, REYNOLDS NUMBER DEPENDENCE AND RELATIONSHIP TO THE LARGE SCALE MOTIONS

Having established the strength of the LSM's in the outer part of the boundary layer, we need to determine the strength of the vortex ring-like Typical eddies, to enable a comparison of strengths. We again used simultaneous laser sheet flow visualization and a 4-wire cross-stream vorticity probe, to obtain an ensemble averaged flow field picture of the Typical eddies. We examined this flow field at the same four Reynolds numbers. Results indicated that non-dimensionalization by the free stream velocity and momentum thickness also successfully collapsed the eddy signatures over the RTHETA range. Fig. 23 shows the zonal decomposition used, and a set of the zonal averages for the normal velocity component. Fig. 24 shows the vorticity and the resulting flow field. We see that the overall direction of motion is away from the wall. Although these Typical eddies were sampled in the outer region, we expect those found in the log region would be similar.

These results enabled us to answer the two remaining questions of the last section. First, as mentioned above, the Reynolds number dependence was removed by outer variable non-dimensionalization as it was for the large scale motions. This was a surprise, because of the known Reynolds number dependence of the <u>length</u> scales of the Typical eddy (Ref. 17),

and may only hold over the limited range of Reynolds numbers so far covered. The dotted lines in Fig. 21 and 22 show the scaled Typical eddy signatures, where the ensemble averaged Typical eddy signature has been positioned at the upstream boundary of the large scale motion. Comparing the velocity components, the Reynolds stresses, and the vorticity content, we can see that the strength of the two motions is very comparable. This data comparison, which is the result of a major effort during the last 3 years, is direct evidence that the large scale motions can play an <u>important</u> role in the turbulence production process. The reason is that their presence can significantly perturb the paths of the Typical eddies in the wall region, thus helping to determine whether a Type 1, 2, 3, or 4 interaction occurs! However, it must be pointed out that this data was taken in the outer part of the boundary layer, and that the influences have been reasonably extrapolated. To obtain a detailed quantitative relationship for both motions in the inner region, we must have better illumination. This is needed for more precise understanding, for future modeling, and as an aid to logically designing an engineering turbulence drag modification device. With our new Copper Vapor laser (June 84) we will have these capabilities. It should be noted that the data contained in Fig. 21 and Fig. 22 has long been sought after to form the basis of an entrainment model of the turbulent boundary layer.

1.8 APPLICATION OF HOT-WIRE DETECTION TECHNIQUES

Studies have been initiated to determine whether some of the commonly used turbulence detection techniques are detecting the turbulence production process. The published techniques studied are due to Blackwelder and Kaplan (Ref. 18), and Zaric (Ref. 19). The technique of Ref. 18 which is called VITA, has been used on our data base with a wire at $y+ = 16$. Fig. 25 shows an instantaneous comparison of VITA detections, and the actual presence of high Reynolds stress. Typically, while some large uv peaks were detected, at least an equal number were not. Furthermore, the detections of the Reynolds stress signals greater than one standard deviation were poor. Fig. 26 shows the dependence of the number of detections on threshold, and the non-dimensional window size. It strongly depends on both. If the threshold is set high, the dependence on window size is reduced. When the threshold is greater than 1.1, VITA is detecting the Typical eddy induced upward moving wall layer fluid, which is at the downstream boundary of the pocket during stage IV (Fig. 4). This study reinforces our earlier conclusion (Ref. 1) which showed that when the detecting wire is at $y+ = 15$ VITA detected only 2-5% of the uv signal when it was so restricted. However, as Fig. 4 indicates, other stages of the production process are equally important, and contribute far more uv to the total Reynolds stress than VITA detects.

We have also tested the detector of Ref. 19. Zaric's detector appears to sense many other phases of the turbulence production process. It detects the pocket in almost every one of its stages. Results, so far, are very encouraging. We hope that it may prove to be a good turbulence detector. Fig. 27 (taken from Ref. 20) shows that it results in wall layer scaling. Furthermore, it is only 40% different from the measured pocket frequency, as compared to 1000% for VITA.

1.9 PROGRESS TOWARDS AN OVERALL MODEL OF THE PRODUCTION PROCESS

Having made measurements in all of the important coherent motions of the turbulent boundary layer during the course of this current contract, and having obtained ensemble averages of the important fluid quantities associated with these motions over four Reynolds numbers in several instances, we are in a position to add detail and partially quantify the interactions that result in the production of turbulence near walls.

In its barest form, the model reduces the complexity of the turbulent boundary layer to large scale motions, Typical eddies, and the thickness of the viscous sublayer. All other manifestations, such as pockets and streaks only reflect the results of the process. Fig. 28 shows a sketch of these aspects. The model relies heavily upon the information

obtained from the vortex ring/wall layer simulation experiments. Comparisons such as shown in Fig. 13 strongly support the following model. The visual comparisons are very good. Furthermore, although we do not have signatures from the simulation, 'back of the envelop' calculations suggest that the signatures measured in the turbulent boundary layer would be produced by the ring/wall shear layer interaction. (The photochromic technique--used to get the velocity profiles (see Fig. 4)--could be used to quantify this type of information.) Even the details are quite good. As Fig. 16 shows, depending upon the angle of incidence of the ring with the wall, and depending upon the thickness of the wall layer, when the Typical eddy approaches, we can have strong production, or essentially no interaction (anywhere between Type 1 and Type 4). The evidence presented in Fig. 21 and 22 shows that the angle of the Typical eddy can be strongly perturbed by the large scale motions, and thus the strength and phase relationship of the large scale motions to that of the Typical eddies, is an important aspect of the production process. Furthermore, we had earlier evidence Ref. 2 that the passage of a large scale motion can itself modulate the thickness of the sublayer. Since thickness is also a critical parameter, the large scale motions have a further role through this effect.

We will start the model when a weak interaction of Type 2 occurs. In this instance a 'hairpin' vortex is lifted out of

the wall region by the incident Typical eddy. There is a reasonable probability that a new Typical eddy will form from the 'pinched off' hairpin (Ref. 15). Weak interactions of Type 2 will occur when the sublayer is thick, or the incident Typical eddy has less than critical velocity defect, or if the eddy is under a large scale motion, or upstream of a weak large scale motion. When the sublayer/Typical eddy scale is smaller, or the eddy is stronger (has more defect), or is in the large scale sweep caused by a strong large scale motion, we will get a Type 3 or 4 interaction. Type 3 will involve strong mixing in the interior of the flow, while Type 4 will have the strongest sweep and strongest mixing very close to the wall, and hence be responsible for the highest drag. Neither Type 3 or 4 result in another identifiable coherent motion (such as the hairpin which results from Type 2 interactions), but both are responsible for the creation of fine scales of motion, and good mixing.

The model is perhaps best summarized in the form of a space-time sequence as shown in Fig. 29. It shows the paths of three large scale motions and two Typical eddies. Fig. 29a shows a Typical eddy at the upstream boundary of a large scale motion of Class A (called type 1 in Ref. 2). Immediately upstream is another large scale motion of Class A. We can follow the evolution of the Typical eddy through Fig. 29g. It has a Type 2 interaction with the wall region, creates a

hairpin vortex of wall layer fluid, remains 'in tact' and is moved to the outer part of the boundary layer. Meanwhile, the hairpin is lifted up into the log region, 'pinches off' forming a new vortex ring-like Typical eddy. Because of the phasing of the large scale motions, it can move outward and upstream relative to the boundary of the large scale motion until it is in the valley between the large scale motions. Once in the valley, it is moved towards the wall. Depending on the factors mentioned above it can have either a strong or a weak interaction. Table I summarizes the possible occurrences.

Thus, we see that the turbulence production process is intimately connected to the three boundary layer features: the Typical eddies, the large scale motions and the instantaneous thickness of the sublayer.

1.10 TURBULENCE DRAG MODIFICATION

The above model and the data base which underlies it, suggests the following ways in which we could effect a reduction in skin friction drag produced by a turbulent boundary layer.

1. Artificially thicken the viscous sublayer. Riblets effectively do this, and are responsible for 5-10% drag

reduction. In vortex ring/wall shear layer interaction experiments with a ribbed belt (work that is currently underway), we found the stability map was moved to the stable side.

2. Produce smaller Typical eddies for a given average sublayer thickness. The reverse of this happens as the Reynolds number increases. The Typical eddies grow with respect to the sublayer when scaled on wall layer variables, which is consistant with the overall drag increasing faster, after transition to turbulence is complete, than for laminar boundary layer flow as Reynolds number increases further.

3. Interrupt the large scale wallward motions generated by the large scale motions of the outer layer. Outer layer flow manipulators have been hypothesized to do this (Ref. 15).

4. Phase the Typical eddies so that more of them form under the large scale motions rather than upstream of them. Thus, they would be moved away from the wall rather than towards it.

It is believed that techniques can be found to study all of these approaches, although it is expected that the development of these processes will require not only overall drag measurements, but also detailed studies of the mechanistic changes that occur.

1.11 SUMMARY

By correctly separating out the influence of a number of mechanisms, we have arrived at an ordered picture of the production process. The major decomposition of events contributing to the production of turbulence, into Type 1 to Type 4 events, allows us to incorporate all of the known observed features without resorting to the old ideas of the onset of some instability process. The form and strength of the interaction is seen to be strongly coupled to the state of the large scale motions through their net convective action, influencing both the relative convective velocity and the angle of approach. The other critical factor is the local instantaneous thickness of the viscous sublayer. An experimental simulation of the eddy/wall interaction has shown that there is a well defined critical combination of relative convection velocity and ring to wall layer thickness. Numerical simulations have shown that the onset of the strong interaction is essentially governed by two-dimensional mechanisms. If similar sharp boundaries exist between the weak and strong interactions for the real Typical eddies in the turbulent boundary layer, we have interesting possibilities for effecting drag reduction and other modifications, by causing a shift in the balance of events to one side or other of the critical boundaries.

1.12 REFERENCES

1. Falco, R. E. 'The Production of Turbulence Near a Wall', AIAA Paper No. 80-1356, 1980.

2. Falco, R. E. 'Coherent motions in the outer region of turbulent boundary layers', Phy. Fluids, Vol. 20, Part II, pp. S124-S132, 1977.

3. Falco, R. E. 'Structural aspects of turbulence in boundary layer flows', in Turbulence in Liquids, pp. 1-15, ed. by Patterson and Zakin, 1980.

4. Runstadler, P. W., Kline, S. J. and Reynolds, W. C., 'An experimental study of the flow structure of the turbulent boundary layer', Report MD-8, Dept. of Mech. Engrg., Stanford Univ., Stanford, CA, 1963.

5. Kline, S. J., Reynolds, W. C., Schraub, F. A. and Runstadler, P. W., 'The structure of turbulent boundary layers', J. Fluid Mech., 30, 1967, pp. 741.

6. Kim, H. T., Kline, S. J. and Reynolds, W. C., 'The production of turbulence near a smooth wall in a turbulent boundary layer', J. Fluid Mech., 50, 1971, pp. 133.

7. Smith, C. R. and Metzler, S. P., 'The characteristics of low-speed streaks in the near-wall region of a turbulent boundary layer', J. Fluid Mech., 129, 1983, pp. 27.

8. Falco, R. E., 'A Synthesis and Model of Wall Region Turbulence Structure', in Structure of Turbulence in Heat and Mass Transfer, ed. by Z. Zaric, pp. 124-135, Hemisphere Press, 1982.

9. Oldaker, D. K. and Tiederman, W. G., 'Spatial structure of the viscous sublayer in drag-reducing channel flows', Phy. Fluids 20, p133, 1977.

10. Falco, R. E. 'The mechanism of turbulence production near walls', Bull. Am. Phy. Soc. Series II, Vol. 25, 1980.

11. Falco, R. E. and Lovett, J. 'The Reynolds number dependence of sublayer streaky structure', to be submitted to Phy. Fluids.

12. Falco, R. E. and Lovett, J. The relationship between the scaling of localized sublayer flow modules and the streaky structure', to be submitted to Phy. Fluids.

13. Yoda, H. 'Effects of dilute polymer additives on the turbulence structure near a wall', MS Thesis Department of

Mech. Engr. Michigan State Univ., 1981.

14. Alfredsson, Ph D Thesis Royal Institute of Technology, Stockholm, 1982.

15. Falco, R. E. 'New Results, a review and synthesis of the mechanism of turbulence production in boundary layers and its modification.' AIAA Paper No. 83-0377, 1983.

16. Offen, G. R. and Kline, S. J., 'A proposed model of the bursting process in turbulent boundary layers', J. Fluid Mech., 70, 1975, pp. 209.

17. Falco, R. E. 'Some comments on turbulent boundary layer structure inferred from the movements of a passive contaminant', AIAA Paper 74-99, 1974.

18. Blackwelder, R. F. and Kaplan, R. E., 'The intermittent structure of the wall region of the turbulent boundary layer', USC Rep. 5 USCAE 1-22, 1972.

19. Zaric, Z. 'Conditionally averaged patterns of coherent events in a wall-bounded turbulent flow, ICHMT/IUTAM Symposium on Heat and Mass Transfer and the Structure of Turbulence, October 8-10, Dubrovnik, 1980.

20. Zaric, Z., Falco, R. E. and Blackwelder, R. F. 'Detection of coherent structures in visual and multiple hot-wire data in boundary layers', to be published

Order of passage of Large Scale Motions	Thickness of Viscous Sublayer	
	THICK	THIN
Class A followed by Class A	Type 1 or 2	Type 3 or 4
Class A followed by Class B	Type 2 or 3	Type 4
Class B followed by Class A	Type 1	Type 1 or 2
Class B followed by Class B	Type 2	Type 3 or 4

Table I

The effect of the phasing of the large scale motions on the severity of the turbulence production process. Type 4 interaction is most violent; see text.

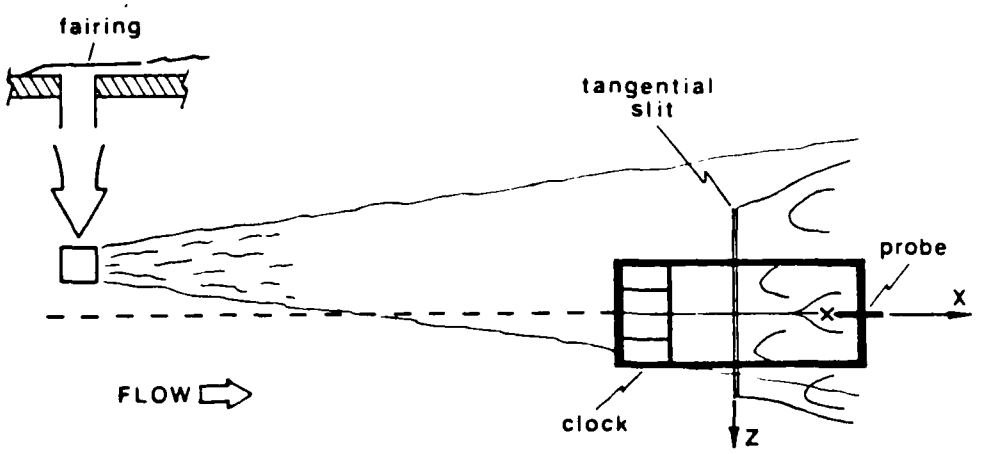

a) Top View or Plan View

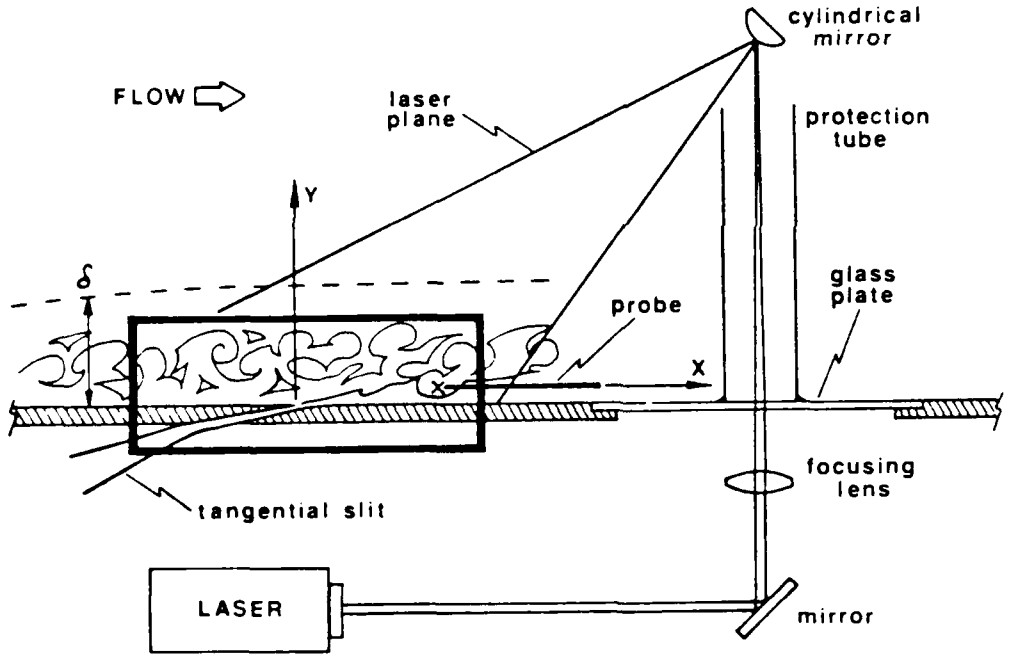

b) Side View of X-Y Plane

Fig. 1 a) Plan view of the two slit technique used, and an example of the field of view with respect to the probe and second slit. b) arrangement used to produce the laser sheet side view.

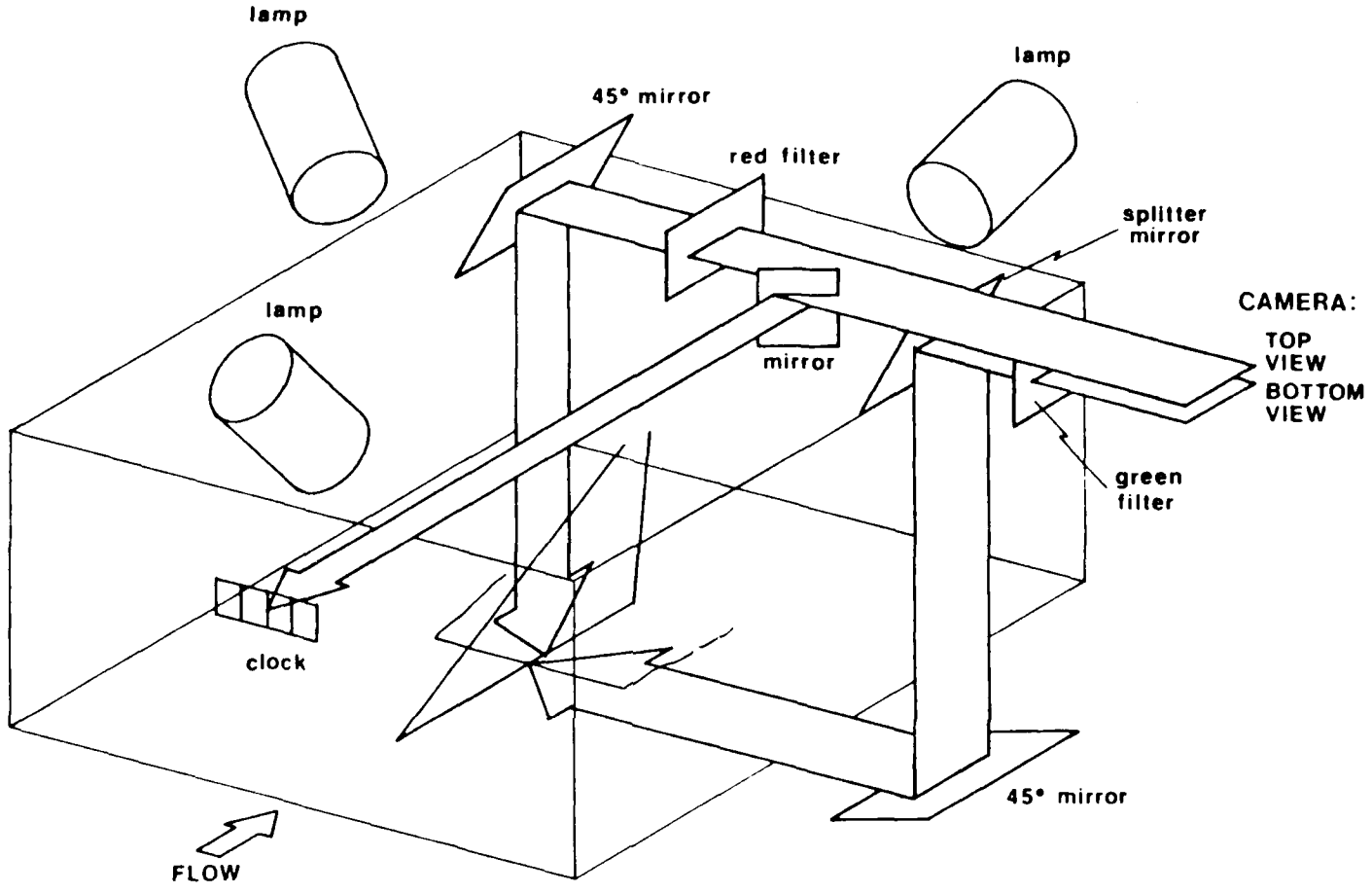

Fig. 2 Mirror and filter and camera arrangement used to obtain the flood illuminated plan view and the simultaneous laser sheet side views.

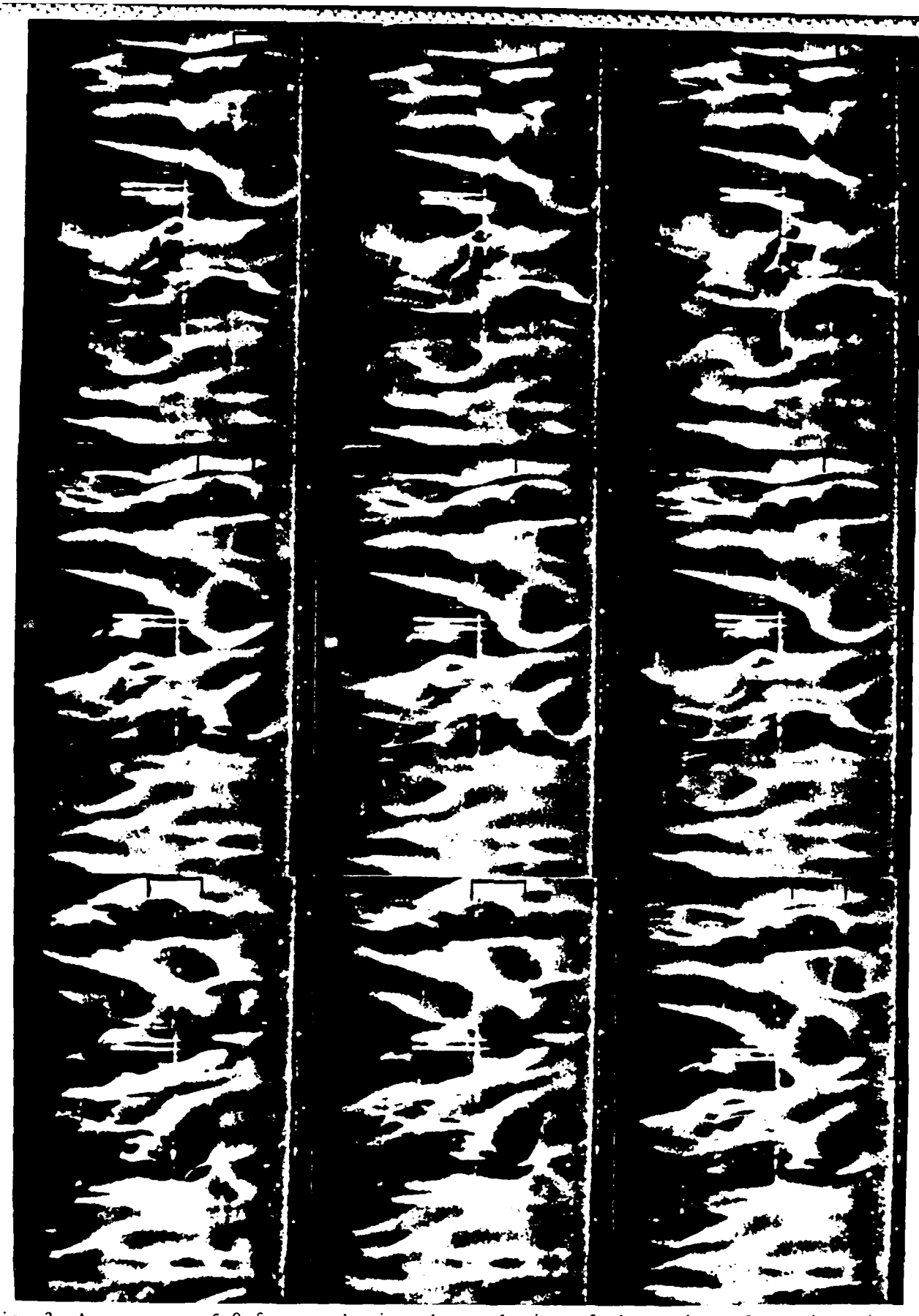

Fig. 3 A sequence of 9 frames showing the evolution of the pocket footprint (one is at the intersection of the brackets, but many more can be seen and followed). Flow is from right to left. A hot-wire probe and digital sequencing counter can be seen.

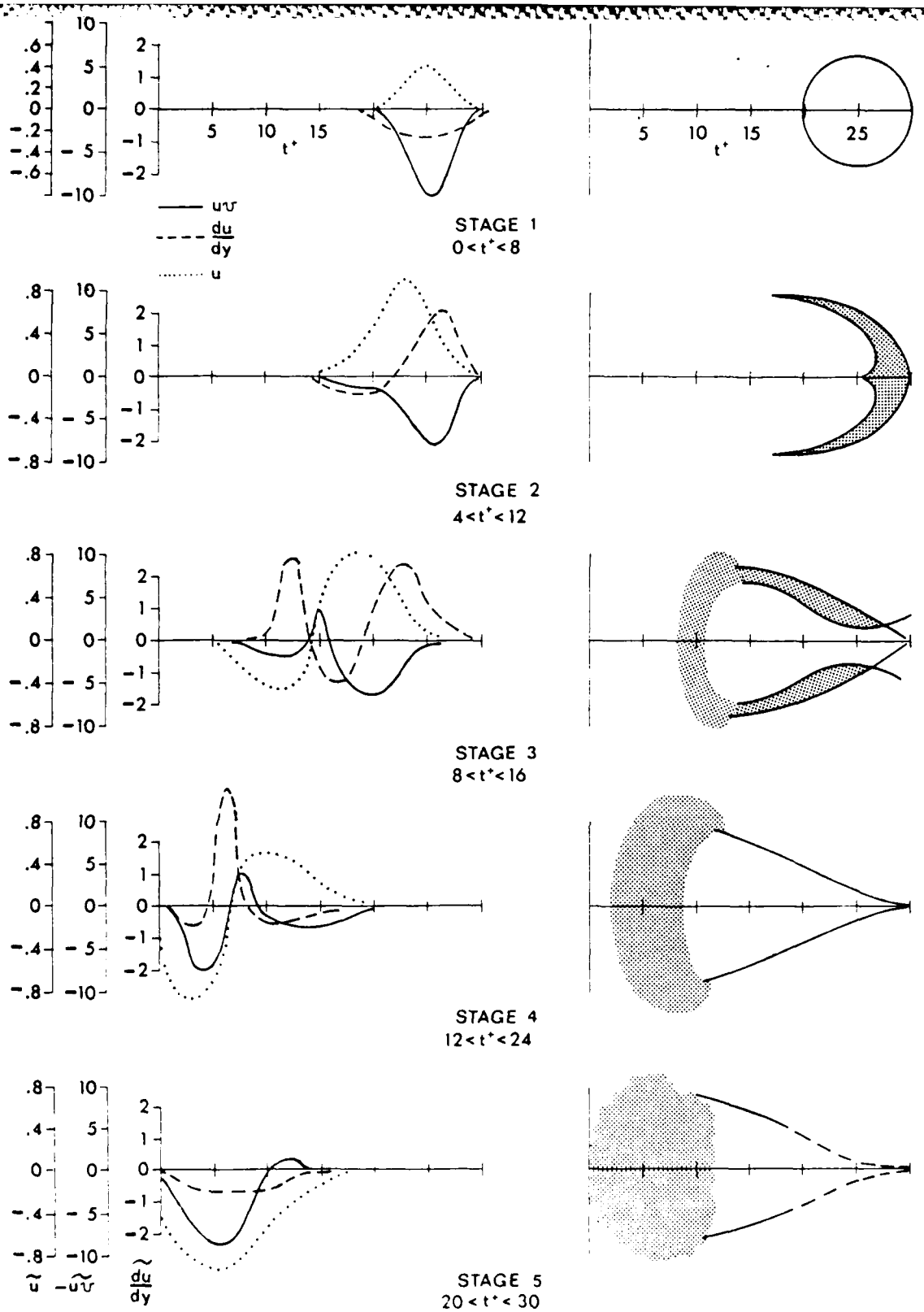

Fig. 4 The evolution of the pocket footprints of the turbulence production process. The plan view pocket patterns and the ensemble averaged signatures of u, uv and du/dy for each of the five stages are shown. In the visual patterns shading indicates lifting fluid. The signals, measured at y+ = 16, indicate conditions along the centerline of the pockets. The visual and hot-wire data have the abscissa scaled identically, and the placement of the signals is phased to the visual pattern, both within each stage and between stages. The ordinates correspond to $(\langle u\rangle - \bar{u})/\bar{u}$, $(\langle uv\rangle - \overline{uv})/-\overline{uv}$, and $(du/dy - \overline{du/dy})/(\overline{du/dy})$. The stages are arranged to show the development an observer would see if he moved with the speed of the upstream end of the visual pattern.

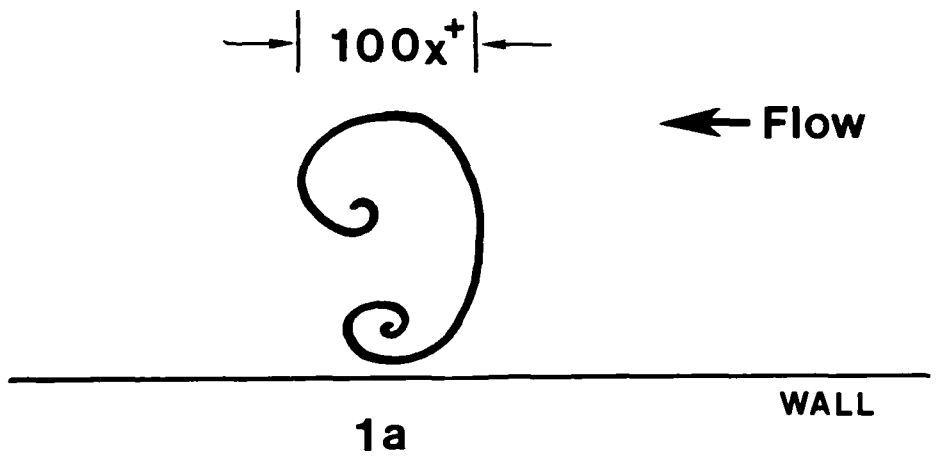

1a

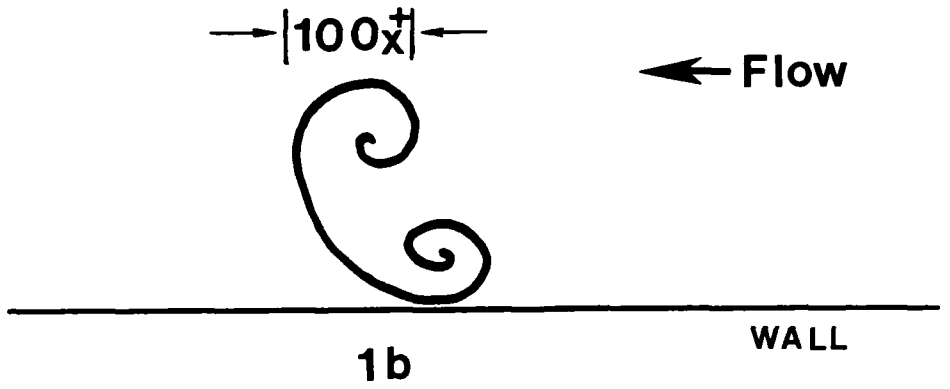

1b

Fig. 5 Two orientations of the Typical eddy. The orientation in 1b is shown in Fig. 6 to be the result of the evolution of a ring of orientation 1a.

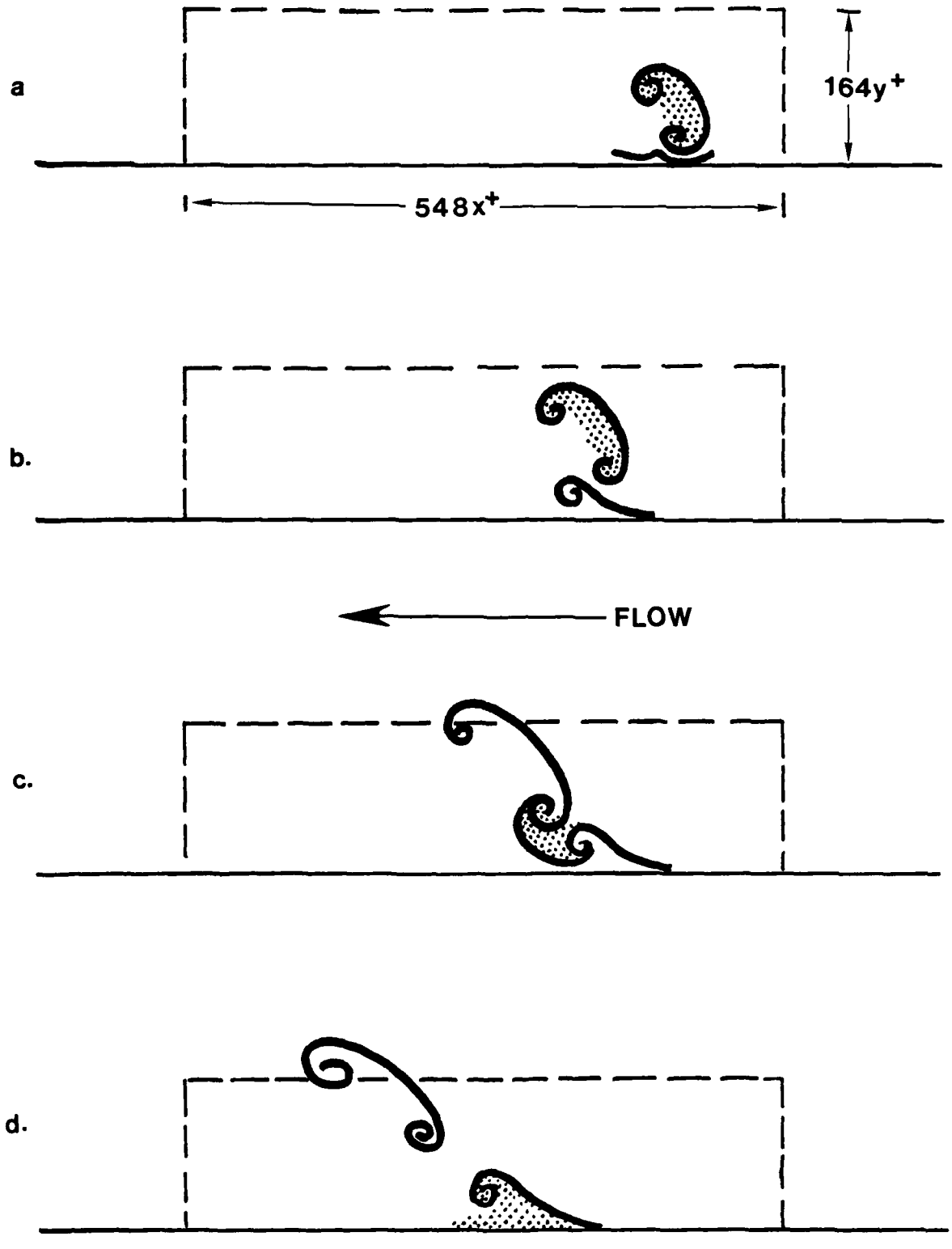

Fig. 6 Four stages in the evolution of a Typical eddy/wall shear layer interaction of Type 1 (see Fig. 8 for summary of all Types). a) Shows a Typical eddy (shaded) approaching the wall; it initiates the pocket and movement away from the wall on the downstream side. b) The Typical eddy moves away from the wall, and the lifted fluid rolls up. c) The Typical eddy convects downstream faster than the roller, and it continues to move away from the wall; the impression in a limited field of view in the laser sheet is that a ring of opposite sign (shaded) exists over the pocket. d) As the Typical eddy moves further away the roller is positioned further upstream of it, and appears as an isolated 'hairpin' at the downstream end of the pocket.

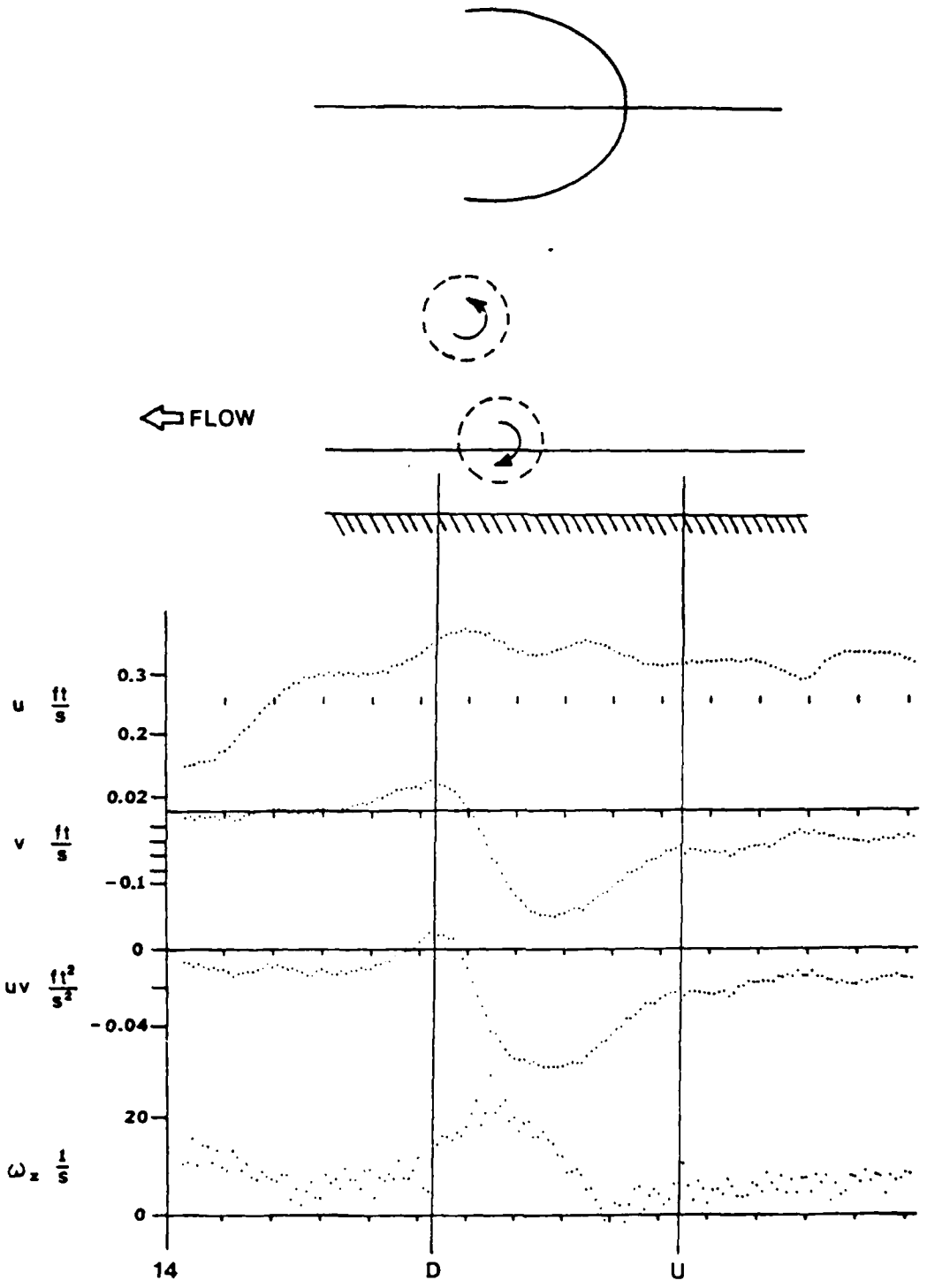

Fig. 7 Ensemble averaged signals of a Typical eddy incident upon the wall region. u, v, uv, and omega z are shown. The Reynolds stress is 6 times the average ambient, and the eddy is in a large scale stream of high speed fluid which is moving towards the wall. We can see that the vorticity of the lower part of the ring-like eddy is strong and positive, in this region where the mean vorticity is -16/sec. This clearly shows that there is significant potential for the ring to induce fluid up away from the wall. In these experiments we did not have probes in the wall region to indicate the thickness of the sublayer, and thus, as we will discuss later, we could not estimate the degree of stretching, and hence do not know whether the strength of vorticity is representative of the maximum or not. Furthermore we did not understand the need to separate the evolutions into the four Types indicated in Fig. 8 at the time this data was taken. We did have a very wide variation in the strength represented in the sample.

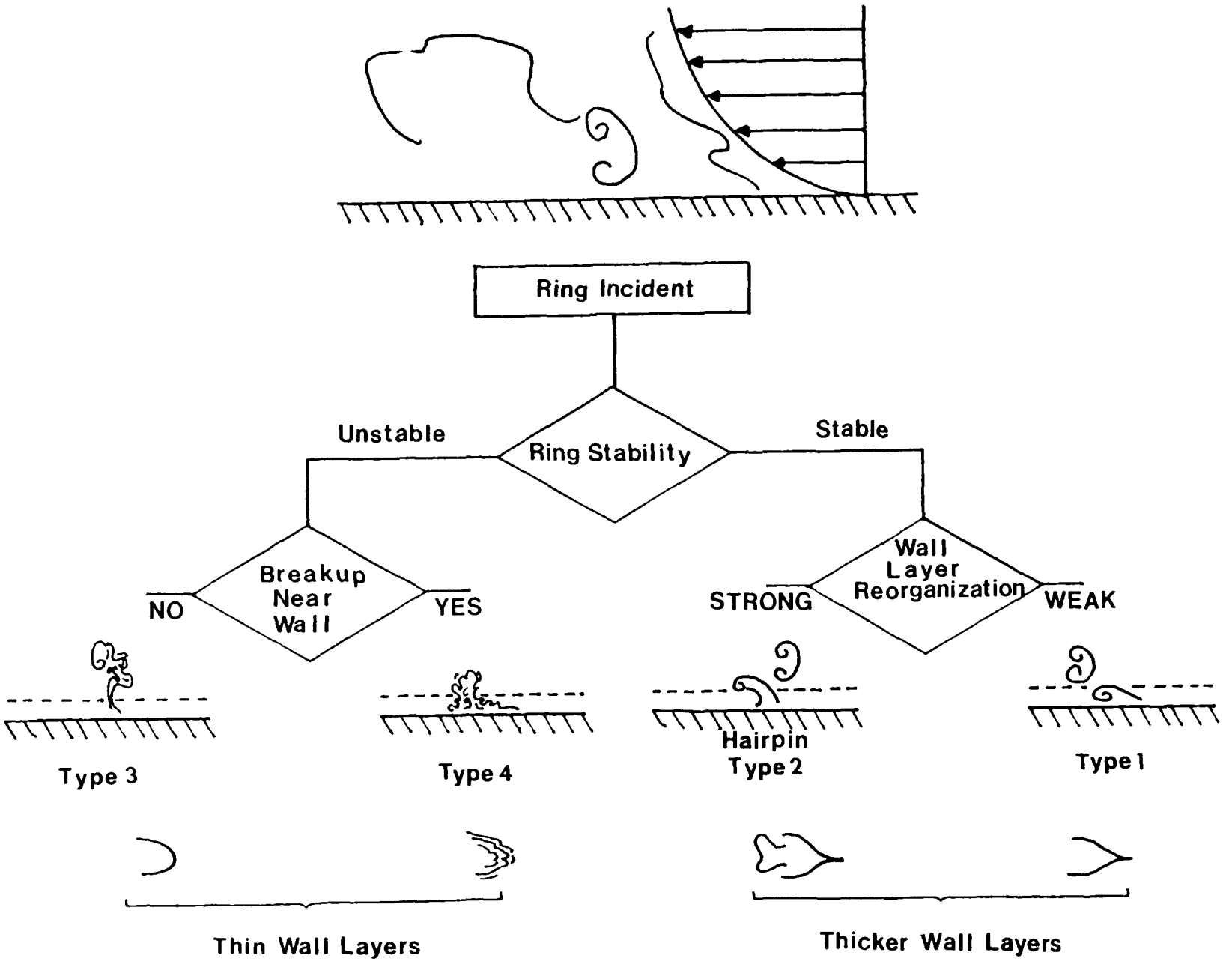

Fig. 8 The four Types of Typical eddy/wall shear layer interactions observed in the turbulent boundary layer when turbulence is produced. Two involve the ring interacting with the wall then leaving the wall without breaking up, and two involve breakup of the ring, and strong mixing, as indicated (see text).

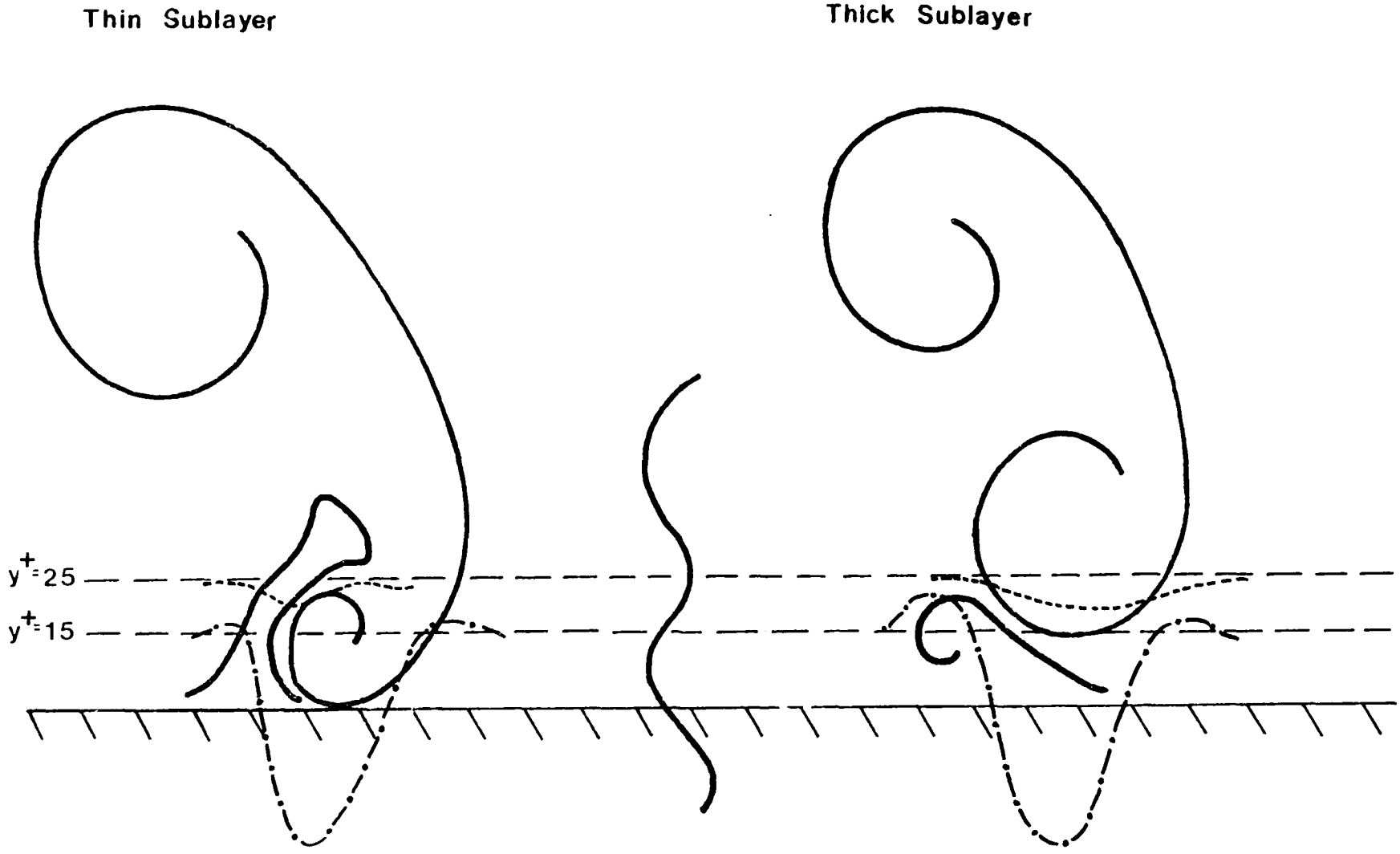

Fig. 9a Because of the small scales of the production events and their high coherency, the signals obtained at different wire positions as the process occurs will be very different. The differences expected at two distances above the wall are shown for uv and omega z in a) and b) -- following page -- respectively. The effect of sublayer thickness on the same strength eddy is also shown. A detector based on magnitude and/or gradients, and located at one position could not incorporate these differences.

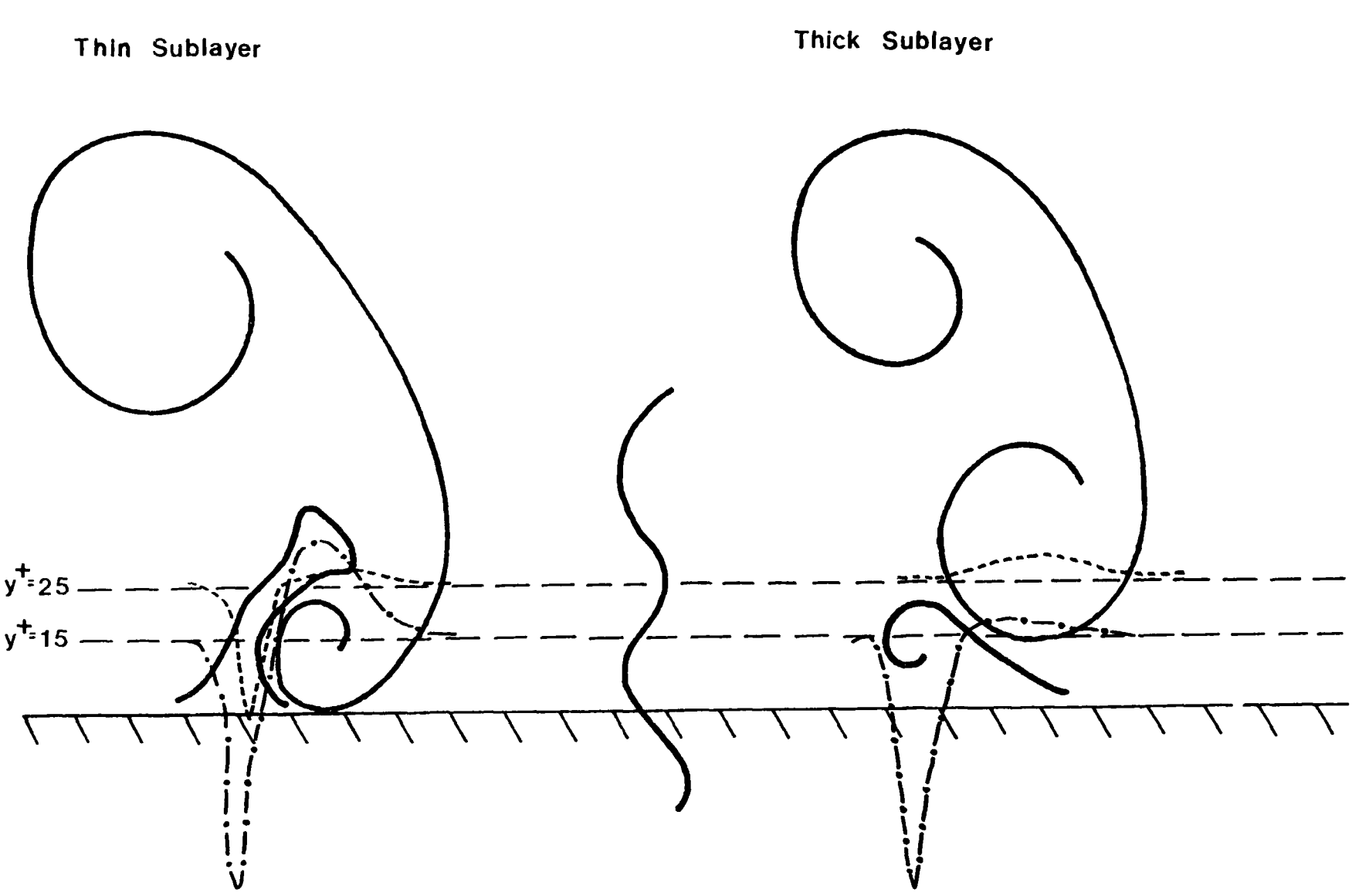

Fig. 9b (see caption on previous page)

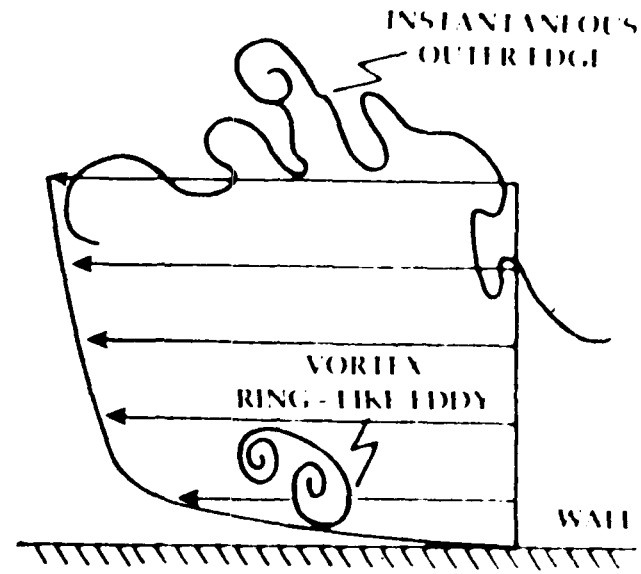

Instantaneous turbulent boundary layer

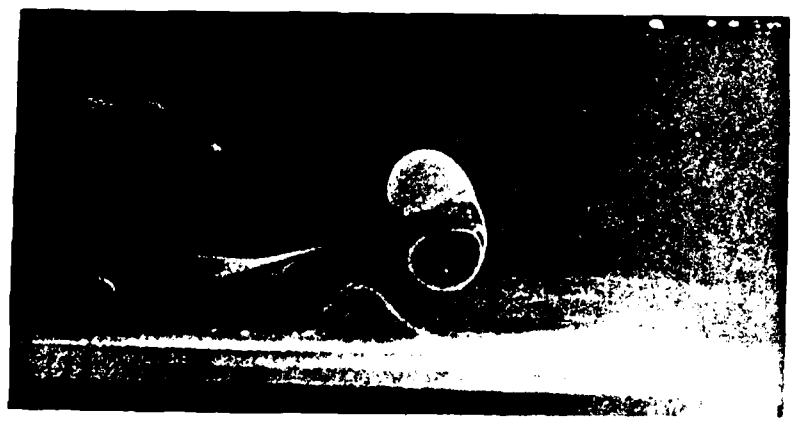

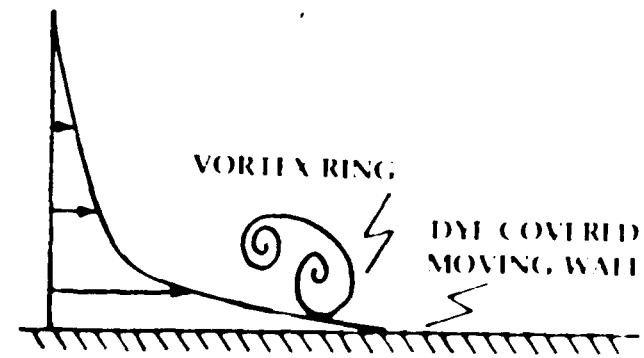

Simulated vortex ring/wall shear layer

Fig. 10 Sketch and photos of the similarity between the Typical eddy in the turbulent boundary layer interacting with the wall layer, and the vortex ring interacting with a moving belt (a Galilean transformation of the ring/wall layer brings it into similarity with the boundary layer interaction).

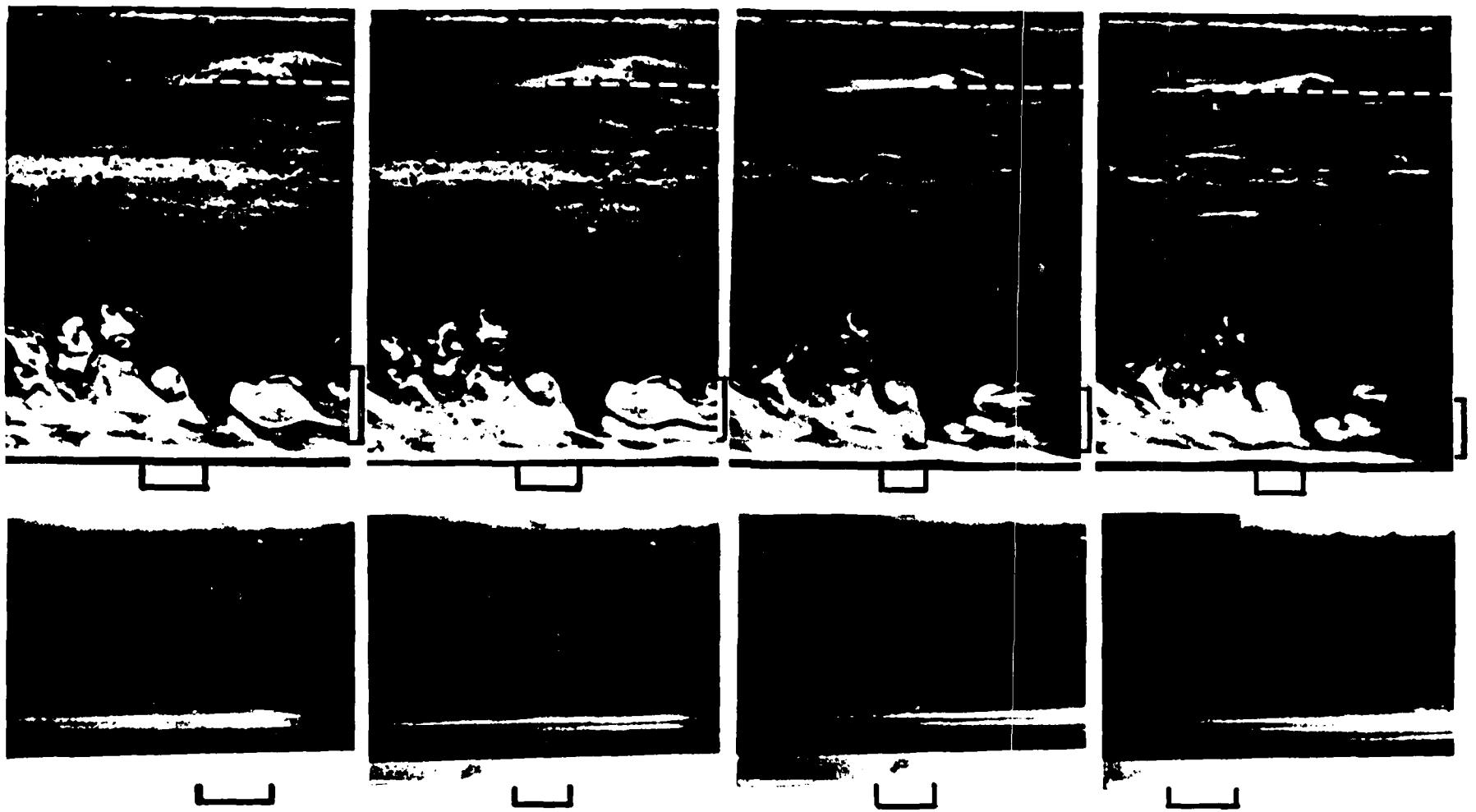

Fig. 11 Sequence showing a Typical eddy interacting with the wall and then leaving without breaking up. It proceeds from left to right. The pocket footprint is also shown. In the lower half, the equivalent ring/wall shear layer interaction. Both are called Type 1 interactions.

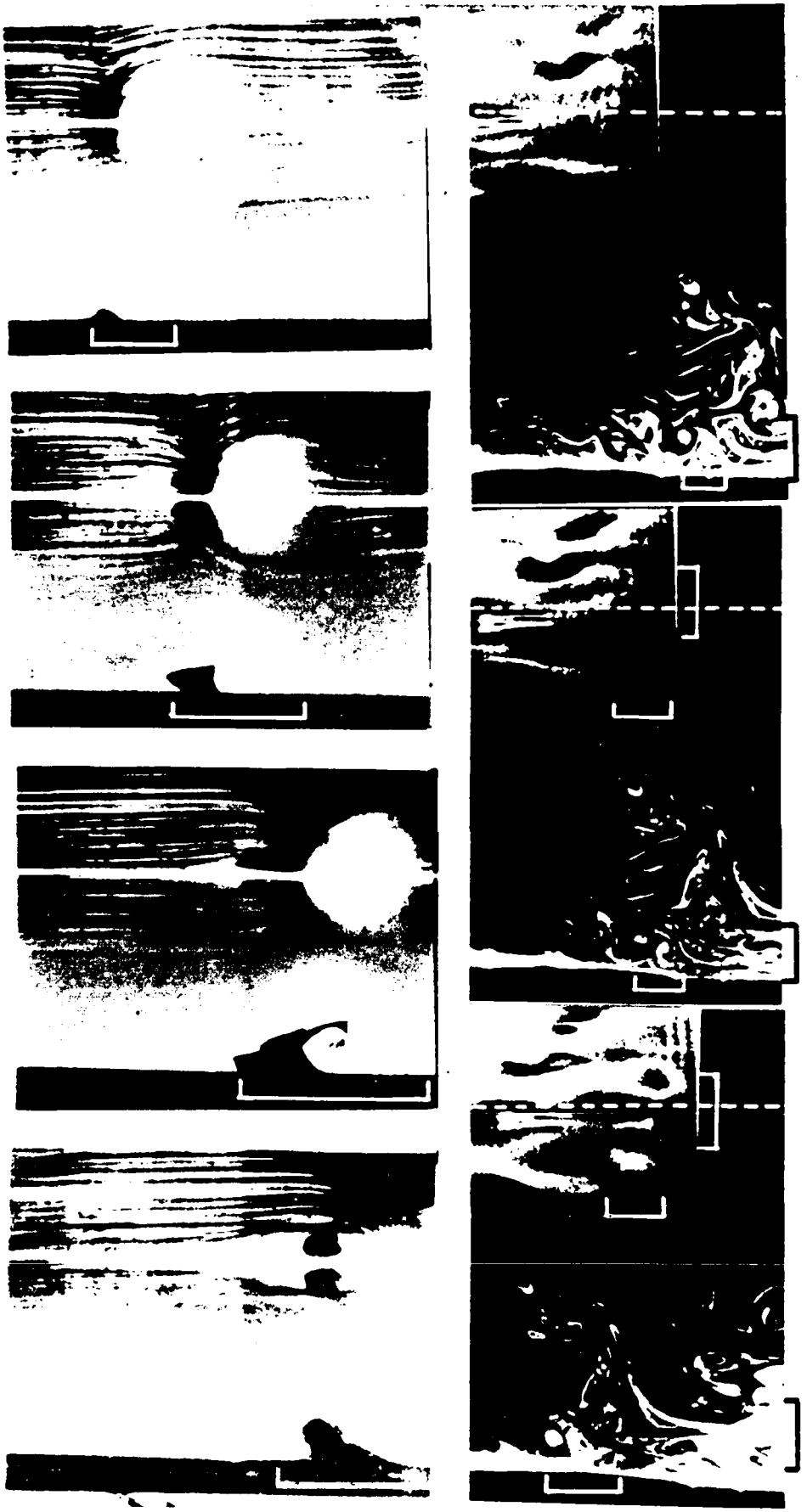

Fig. 12a Type 3 interaction in the boundary layer and in the vortex ring/wall simulation. In both cases, the lower part of the Typical eddy/vortex ring breaks-down as the ring moves away from the wall, after injesting fluid. Boundary layer data on left; flow from right to left.

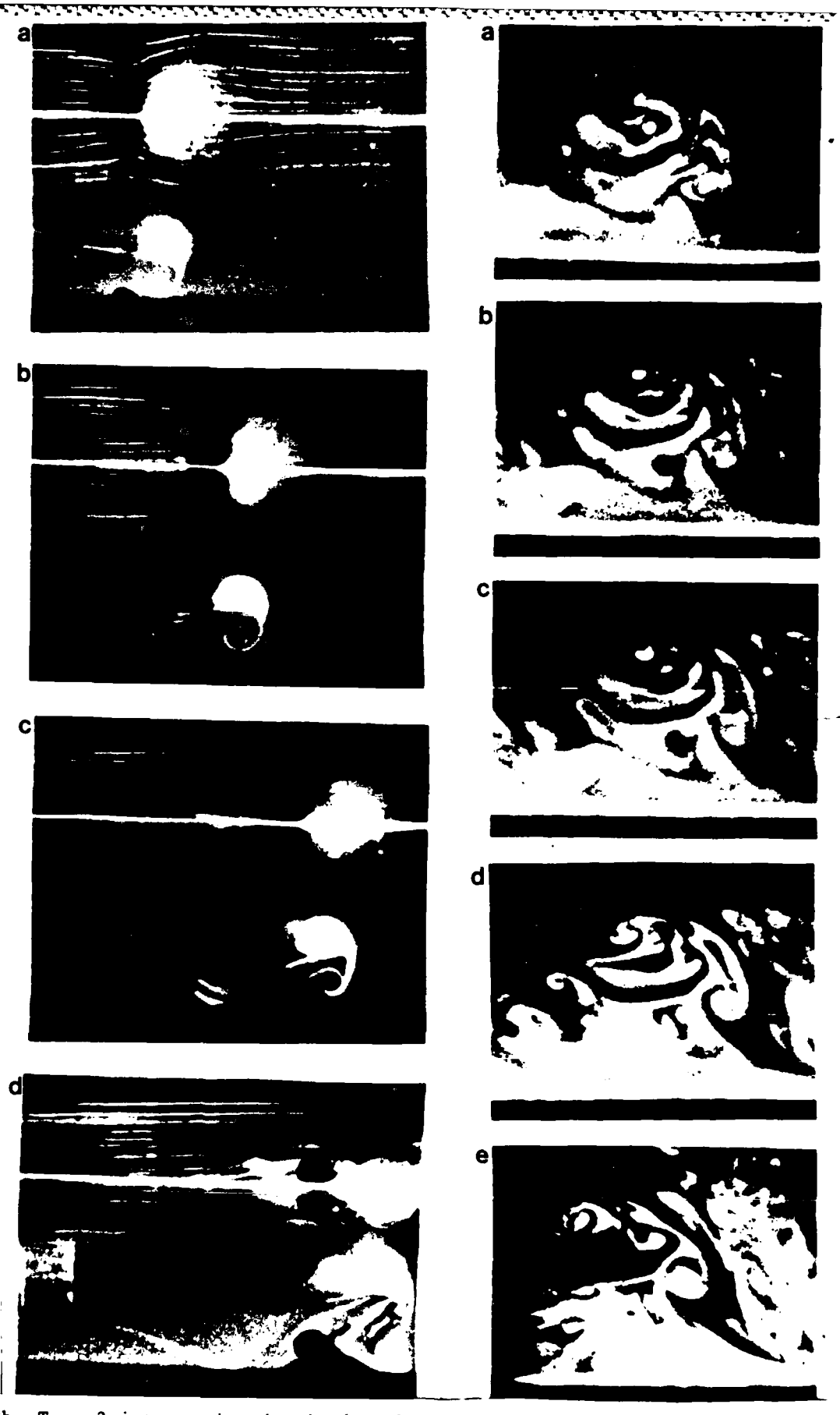

Fig. 12b Type 3 interaction in the boundary layer and in the vortex ring/wall simulation. In this example, we can clearly see the liftup of sublayer fluid into the ring. This fluid takes on the shape of a thumb. After being ingested, the Typical eddy breaks up (differently from the case in Fig. 12a).

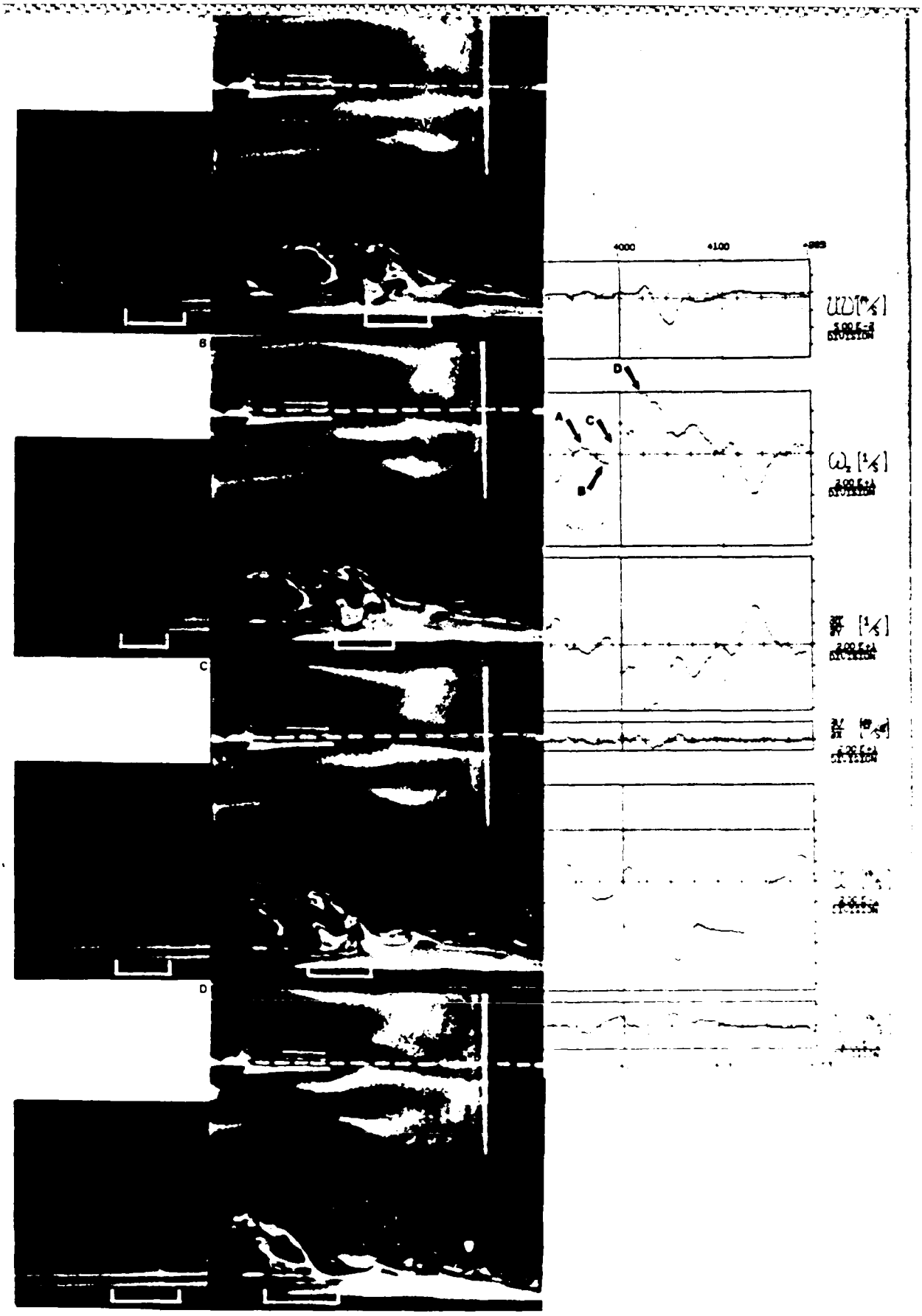

Fig. 13 Type 4 interaction in the boundary layer and in the vortex ring/wall simulation. The Reynolds stress and vorticity which occurred are also shown. The strong increase in the vorticity attests to the stretching of the lower part of the eddy, which is more clearly seen in the ring in part c.

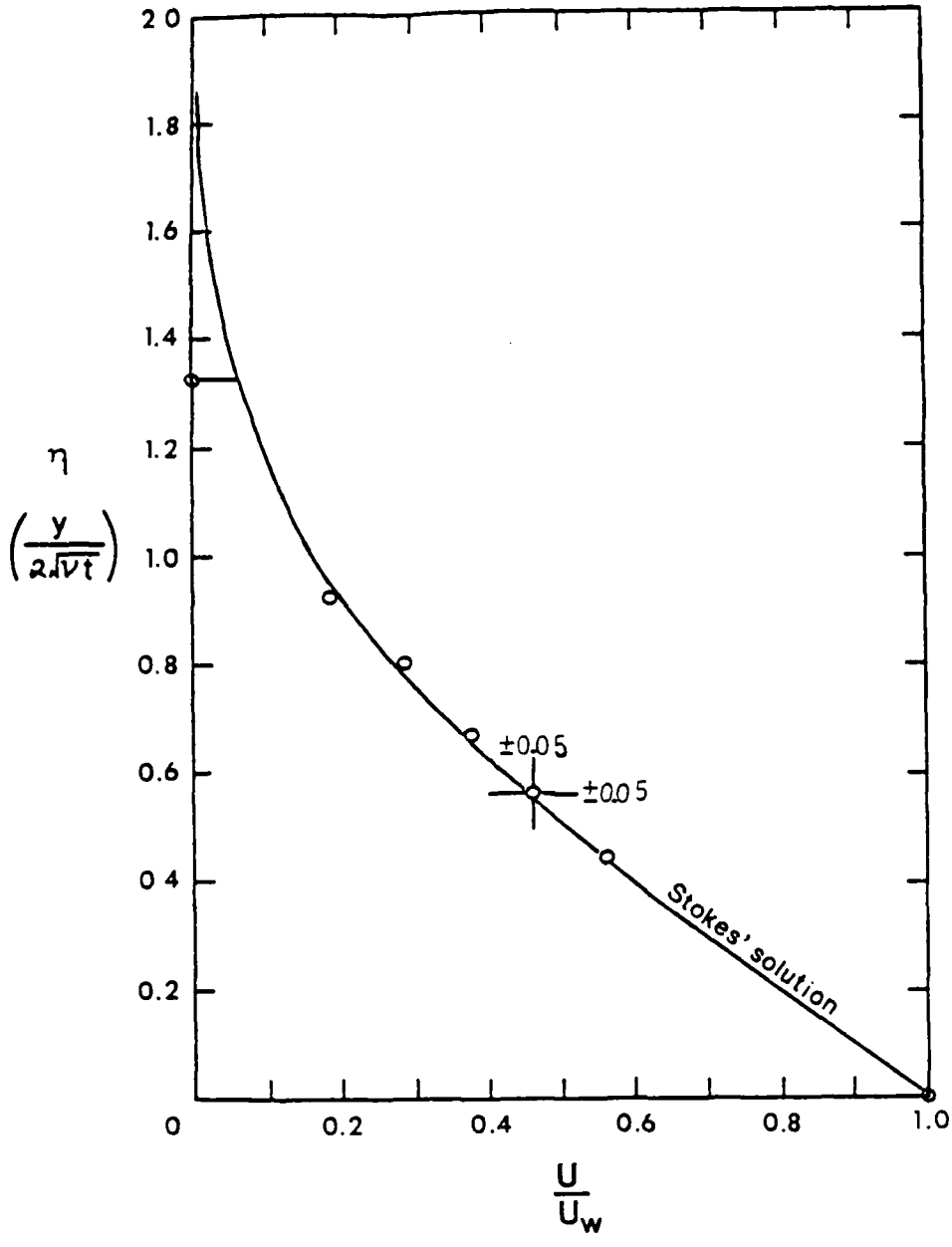

Fig. 14 Velocity profile in the boundary layer on the moving belt. 0 -- experimental data. Solid line is Stoke's exact solution of the Navier-Stokes equations.

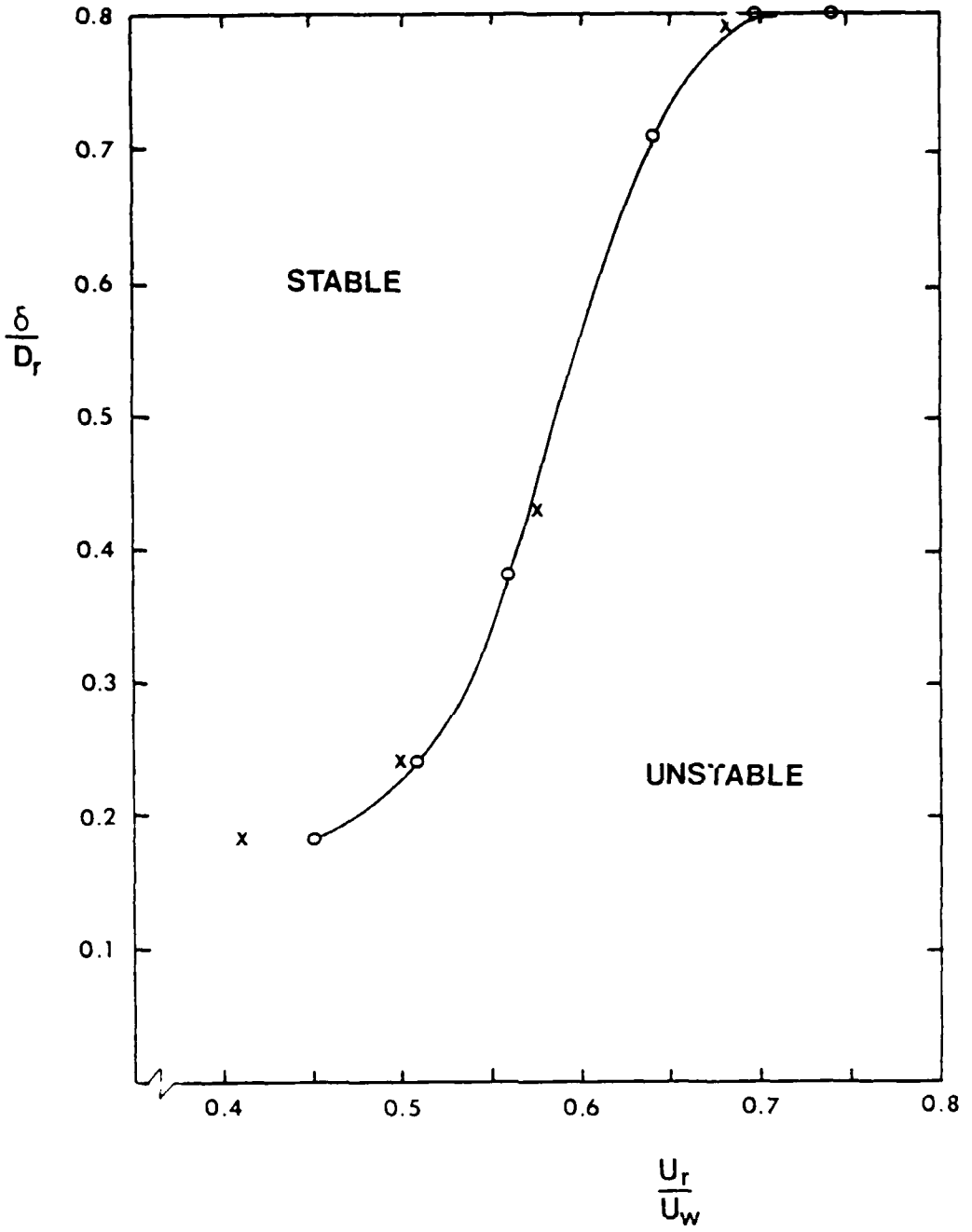

Fig. 15 Parameter map showing the regions of stable interactions, defined as Types 1 and 2, and the regions of unstable interactions defined as Types 3 and 4 -- for vortex rings at 15 degree incidence angle. Data for rings of two different speeds is shown.

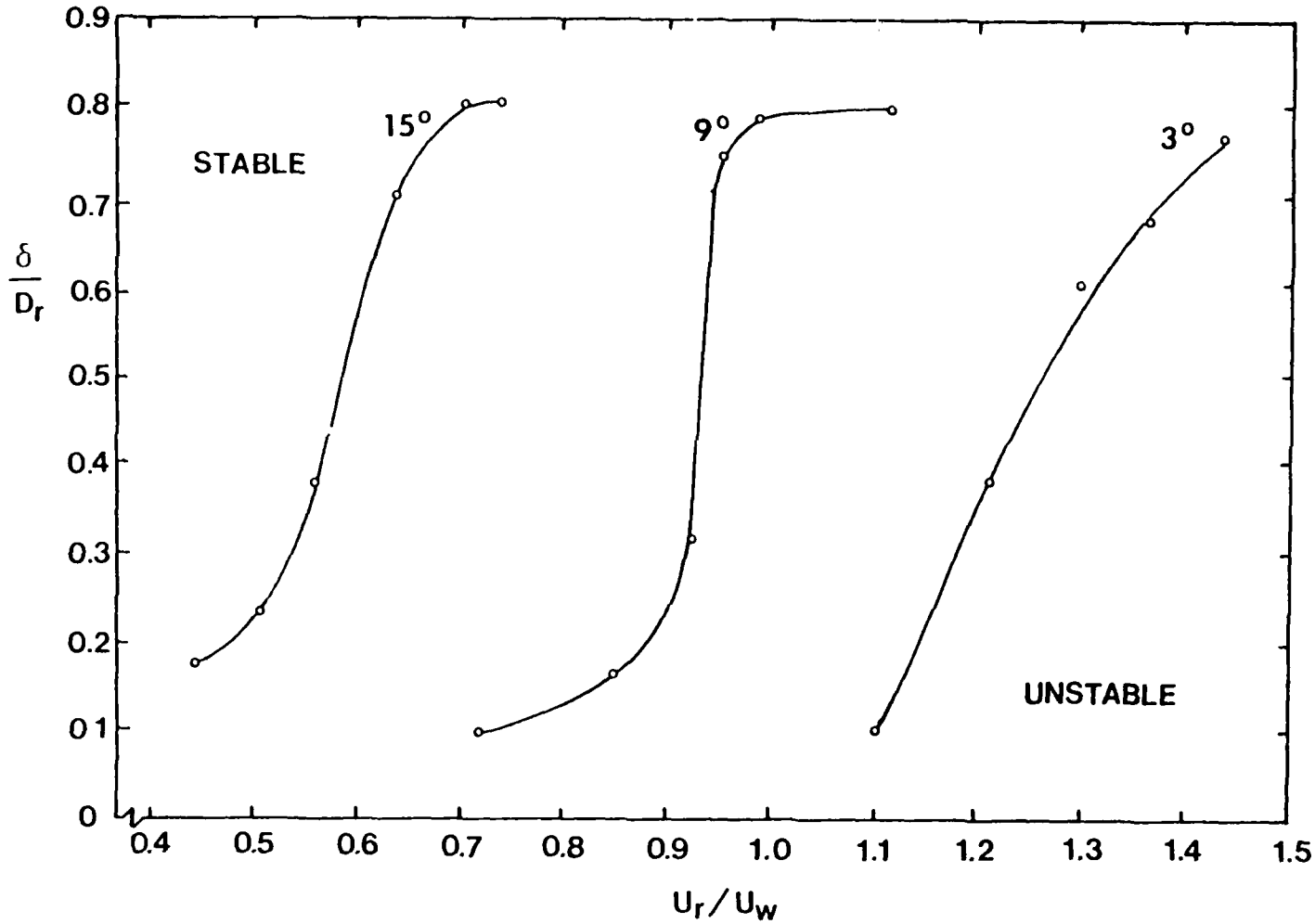

Fig. 16 Stability maps for ring/wall shear layer interactions at incident angles of 3, 9, and 15 degrees. Note the sensitivity to changes in angle.

GEOMETRICAL ARRANGEMENT FOR VORTEX-IN-CELL NUMERICAL SIMULATIONS

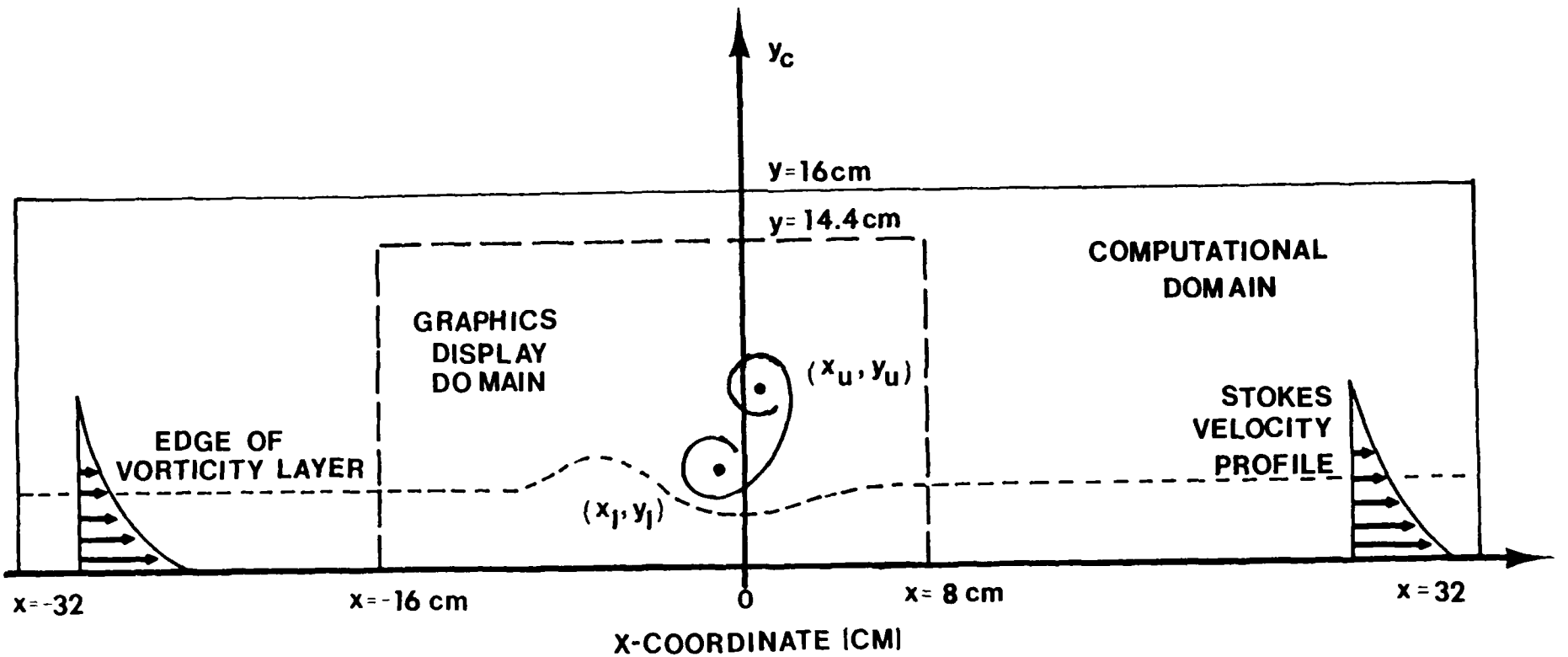

FIGURE 17. Overview of the Computational flow domain showing the graphics display domain (dashed lines). Figures 12 and 13 show only those vortex markers which lie inside this region.

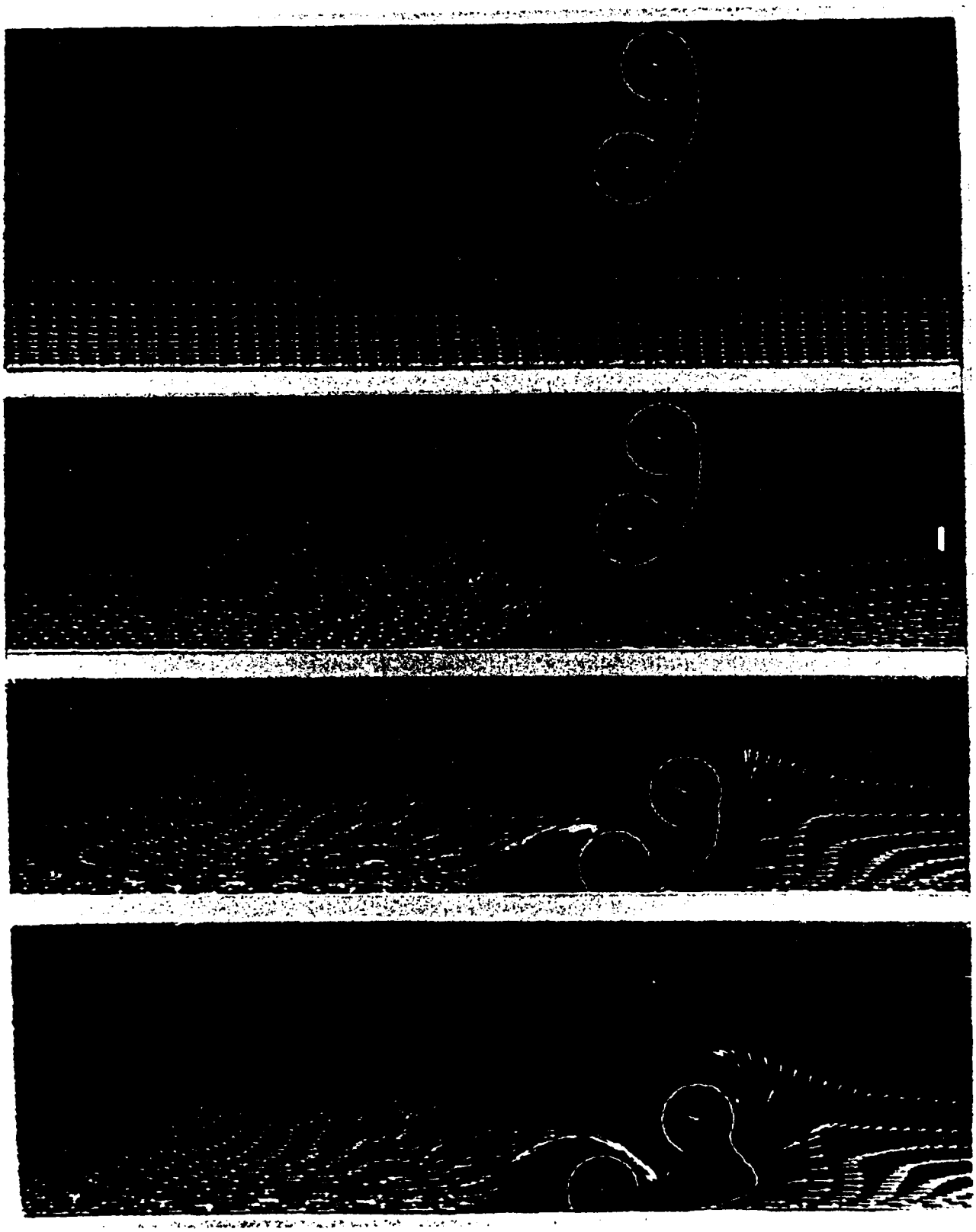

Fig. 18 Two-dimensional numerical simulation of a Type 4 interaction. Note the ingestion of wall layyer fluid into the lower lobe as the line pair approaches very close to the wall. Compare this result with parts (a) and (b) of Fig. 13. Both the line pair and the wall are moving left to right. The outline around line pair is for reference only.

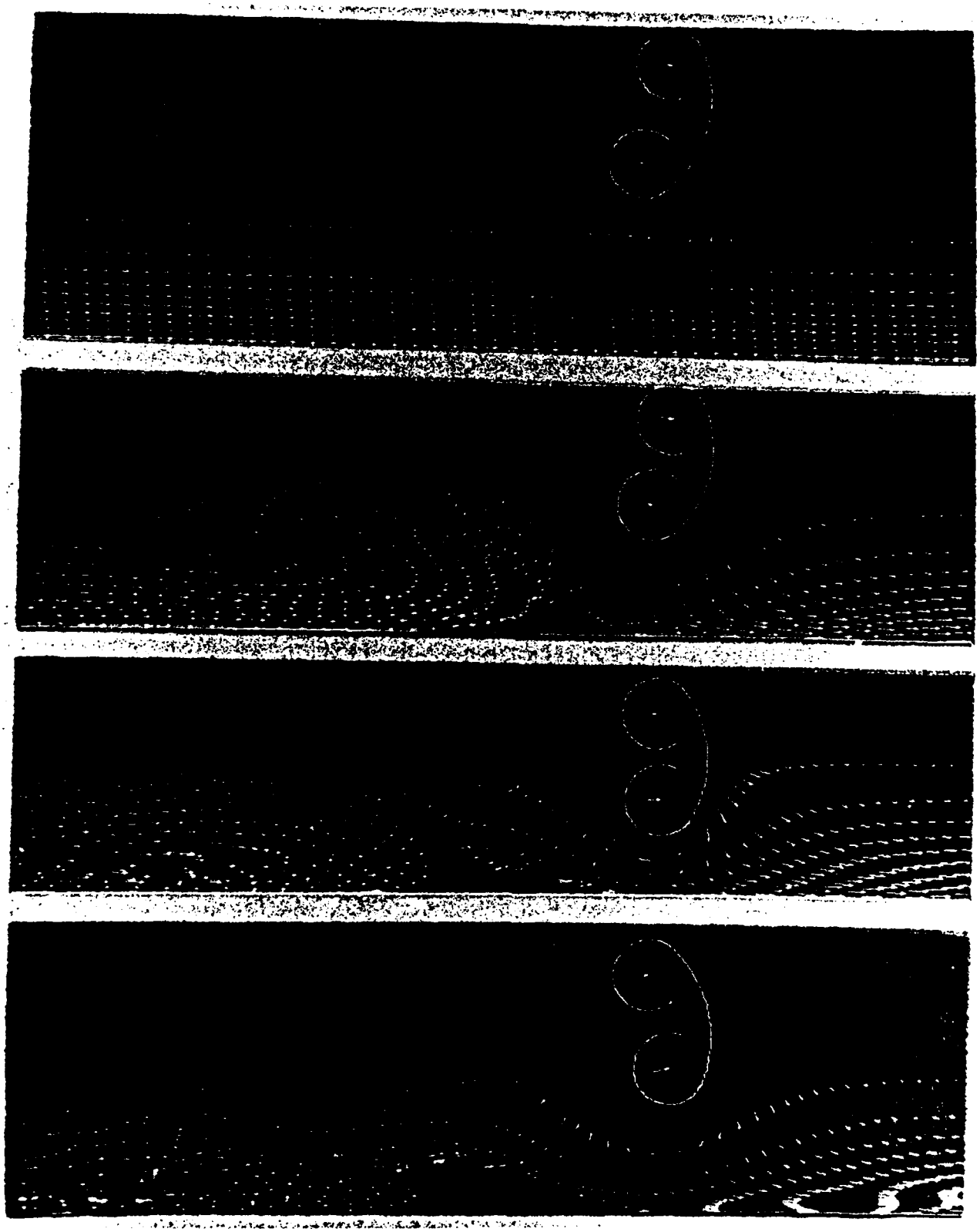

Fig. 19 Two-dimensional numerical simulation of a Type 1 interaction. All conditions are identical to those in Fig. 18, except that the wall layer thickness is less. In this case the line pair leaves the wall region without breaking up. Compare this evolution with the ring in Fig. 11.

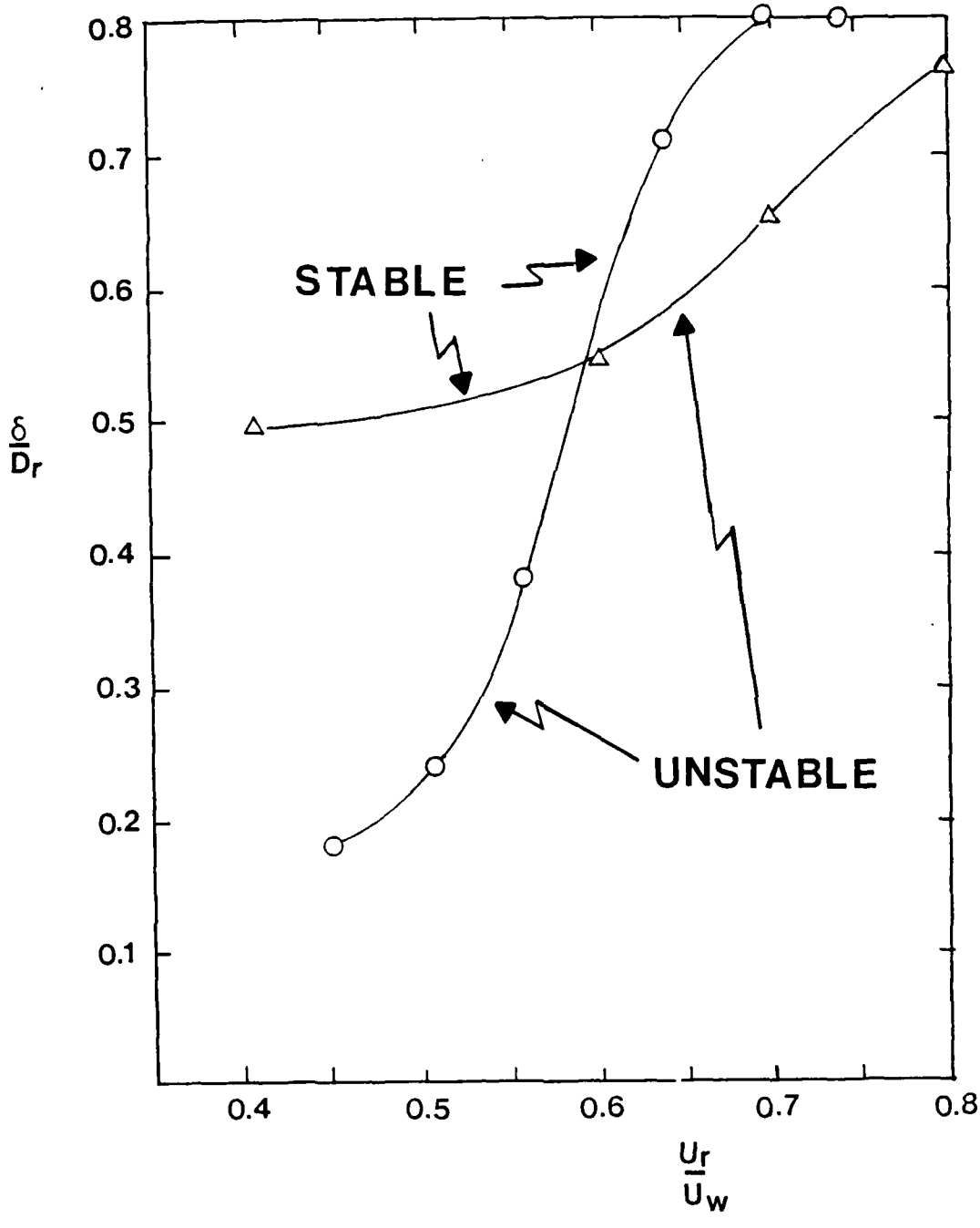

FIGURE 20. Comparison of the non-dimensional stability boundaries for 15° incident rings. O experimental data; Δ two-dimensional computation. Note that the boundary layer thickness, obtained using the photochromic technique, showed a deviation from the Stokes solution used in the computations for $\delta/D_r \geq 0.5$ due to belt leading edge effects.

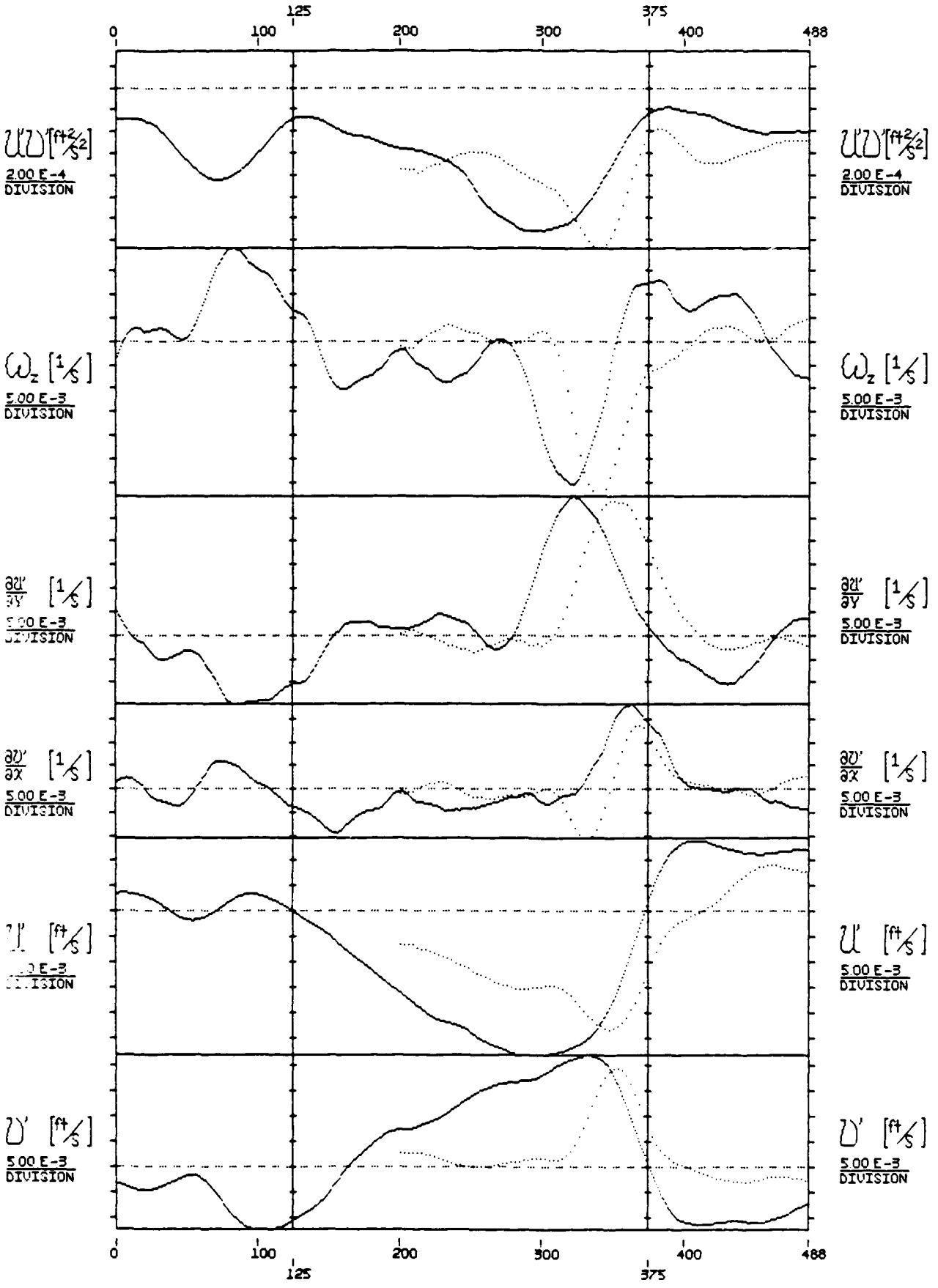

Fig. 21 Comparison of the ensemble averaged large scale motion signatures with those of the Typical eddies, when both are scaled on outer layer cariables. The Typical eddy has been positioned at the upstream boundary of the large scale motion as seen on average in nature. It is clear that the strength of the large scale

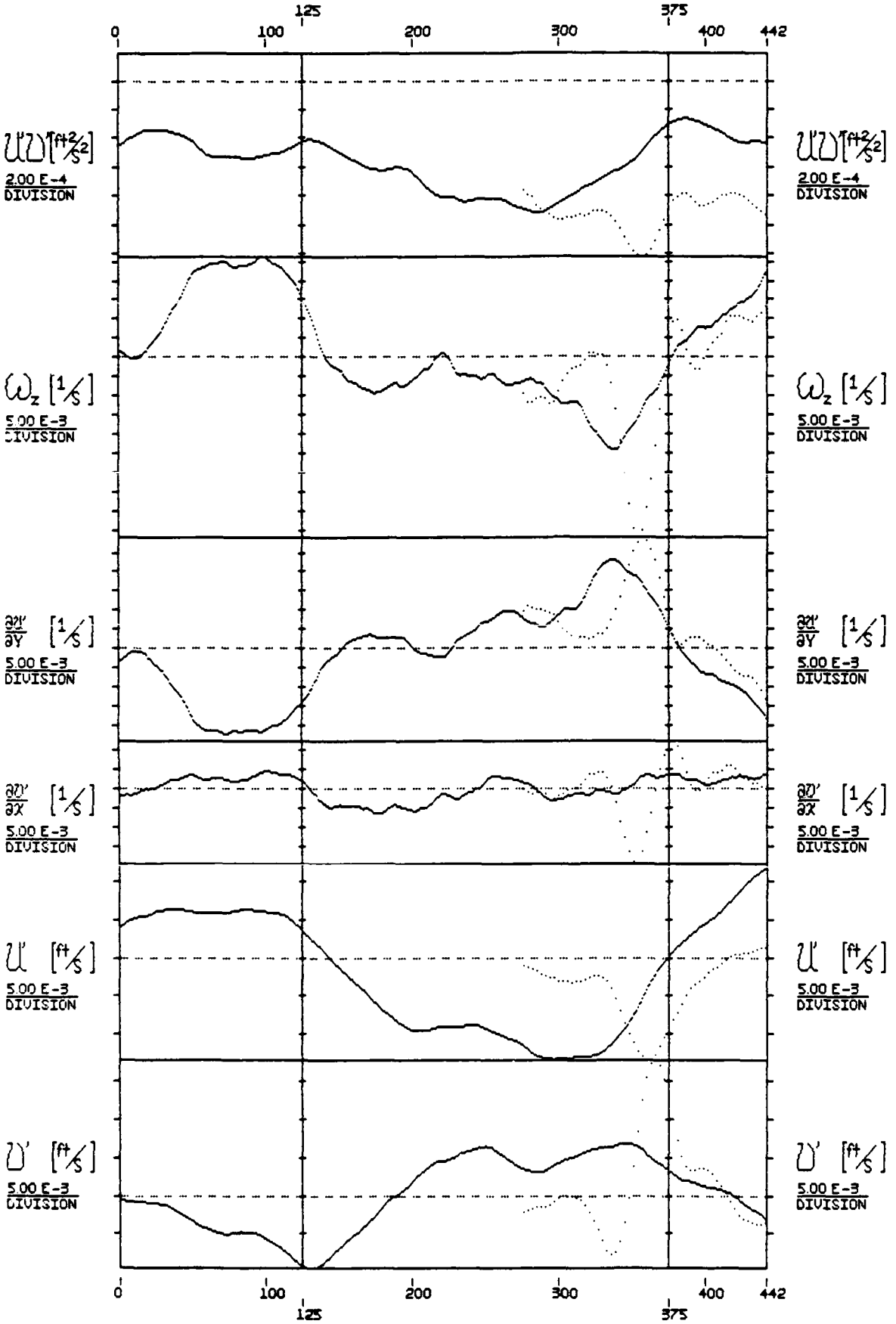

Fig. 22 Comparison of the ensemble averaged large scale motion signatures with those of the Typical eddy signatures at RTHETA = 3116. The strength of the large scale motion remains comparable to that of the Typical eddy.

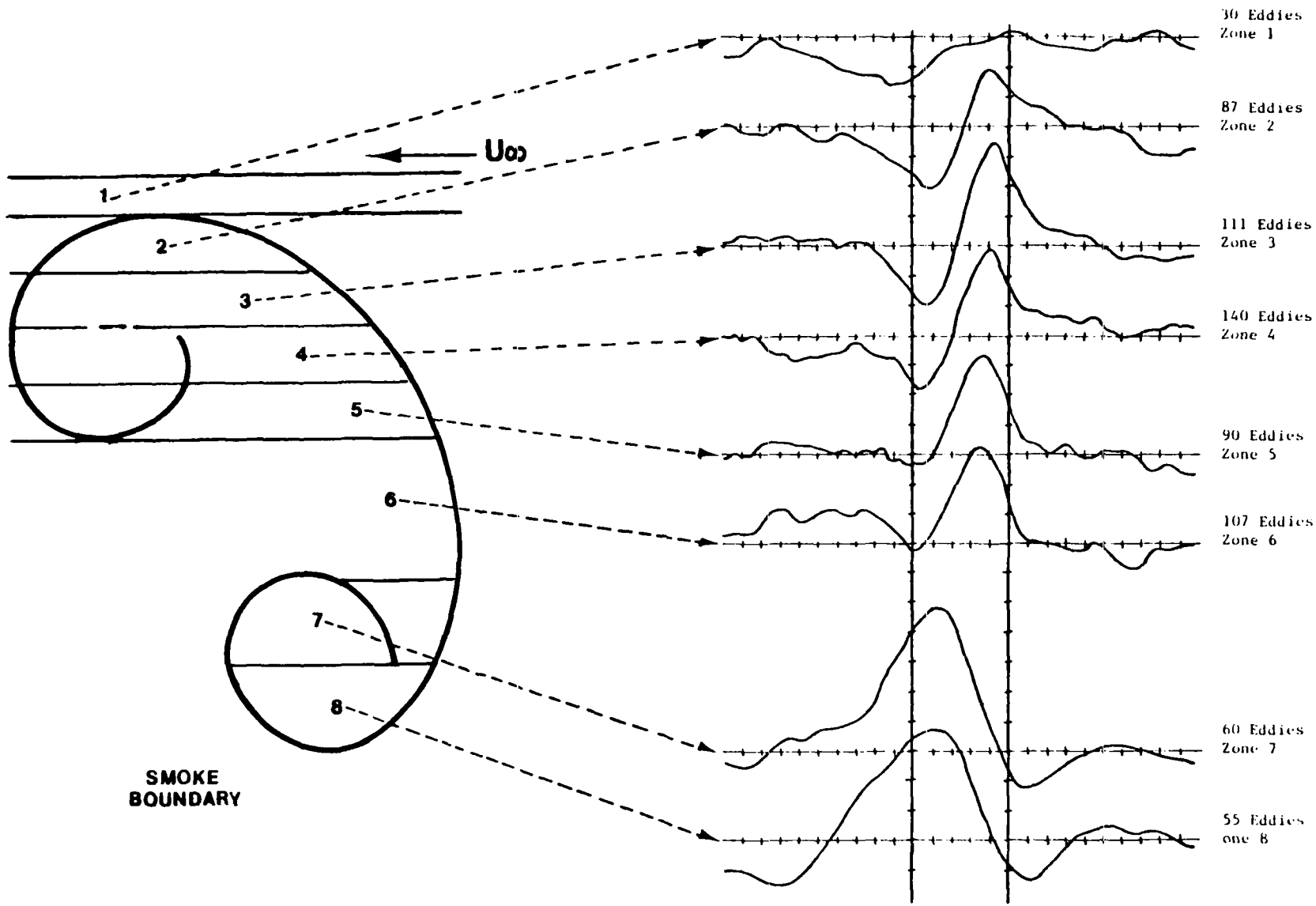

Fig. 23 An example of the breakdown into zones, used to determine the flow field, along with the ensemble averaged normal velocty component.

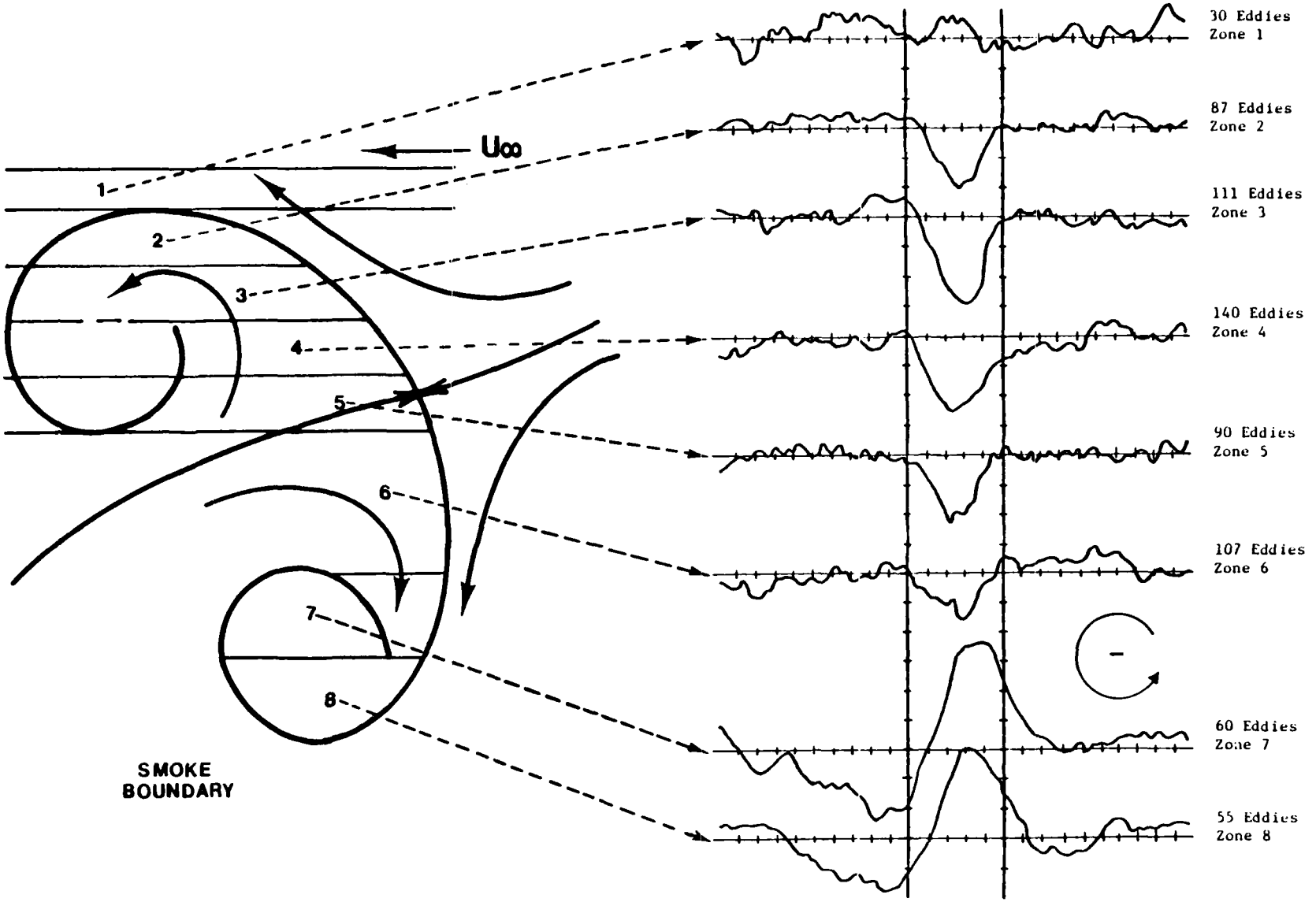

Fig. 24 The flow field derived from vorticity signatures (shown) and strain rate signature (not shown).

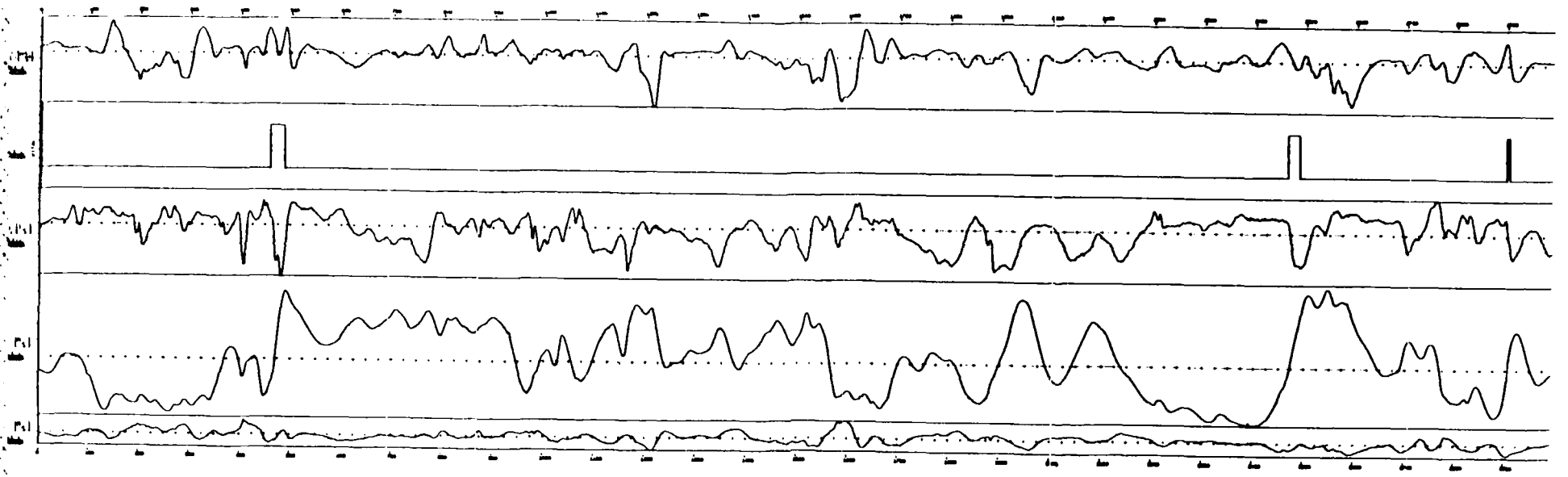

Fig. 25 Simultaneous records of uv, VITA, omega z, u and v, at y+ = 18 (from top to bottom). We can see that there are many large uv peaks that are not detected.

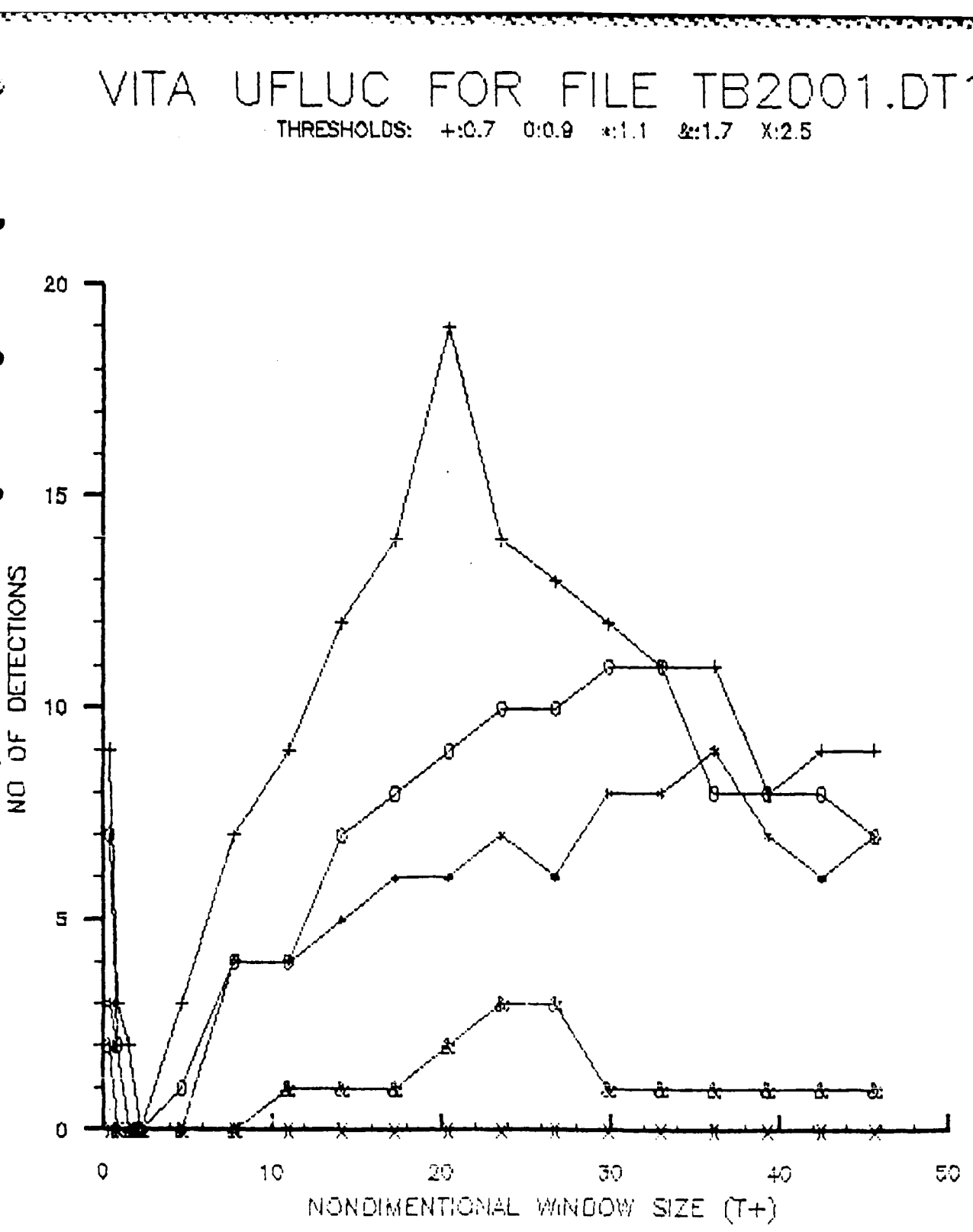

Fig. 26 The number of detections by VITA versus the non-dimensional window size (in wall layer units). Results for several threshold level are included. Note that there does not appear to be any threshold for which the number of detections is independant.

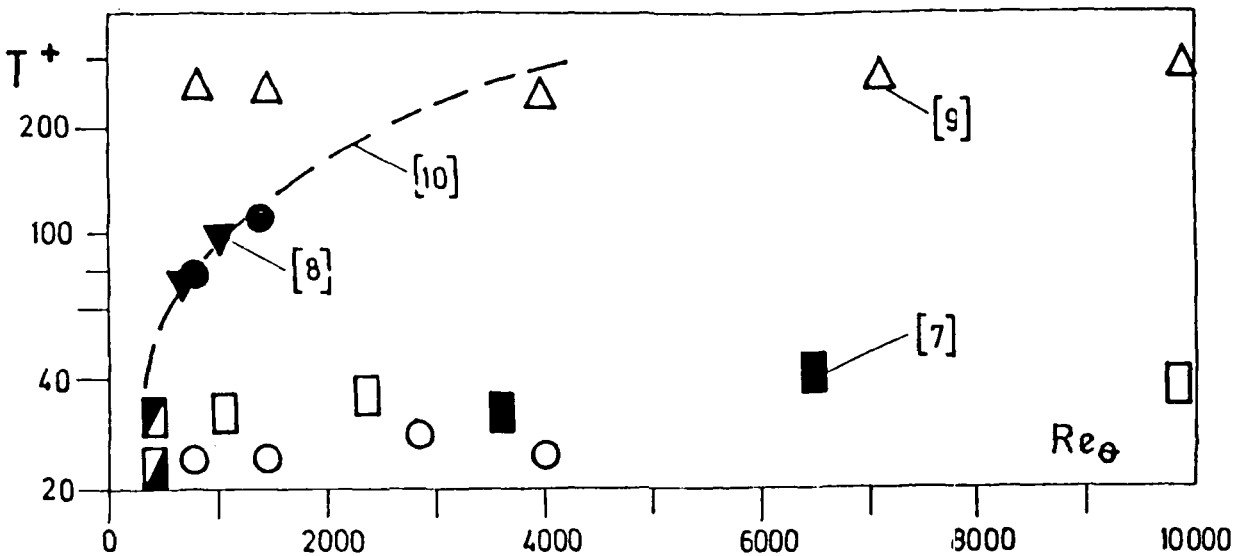

Fig. 27 The period of occurrence new turbulence: ■ Zaric'-Falco; ○ Falco.

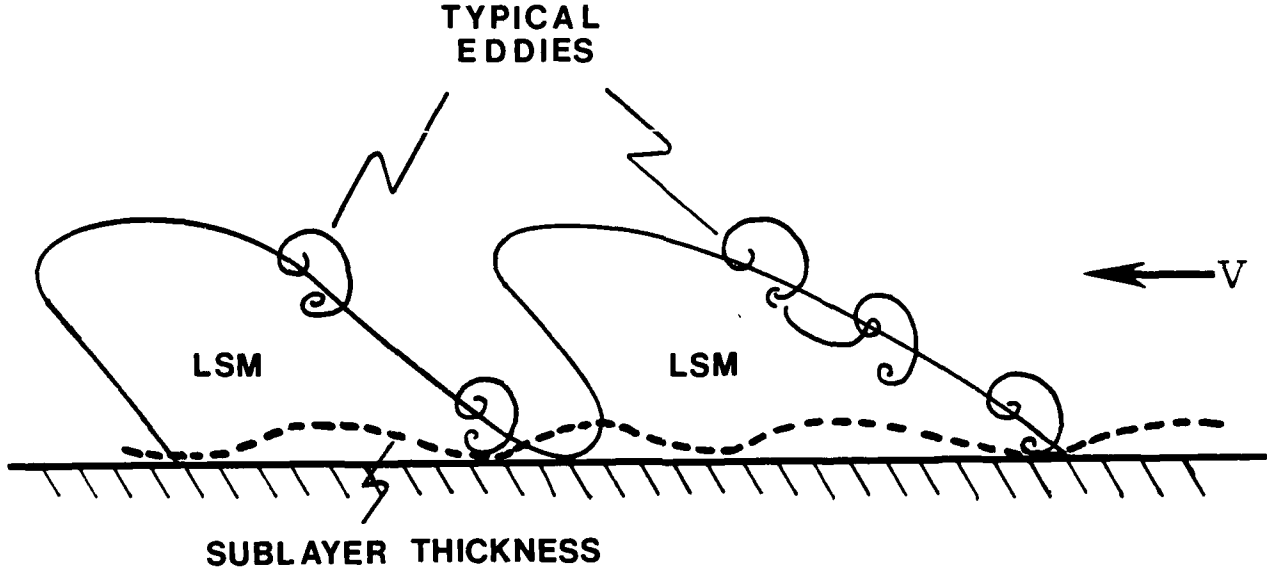

Fig. 28 Sketch showing the three most important aspects of the turbulent boundary layer.

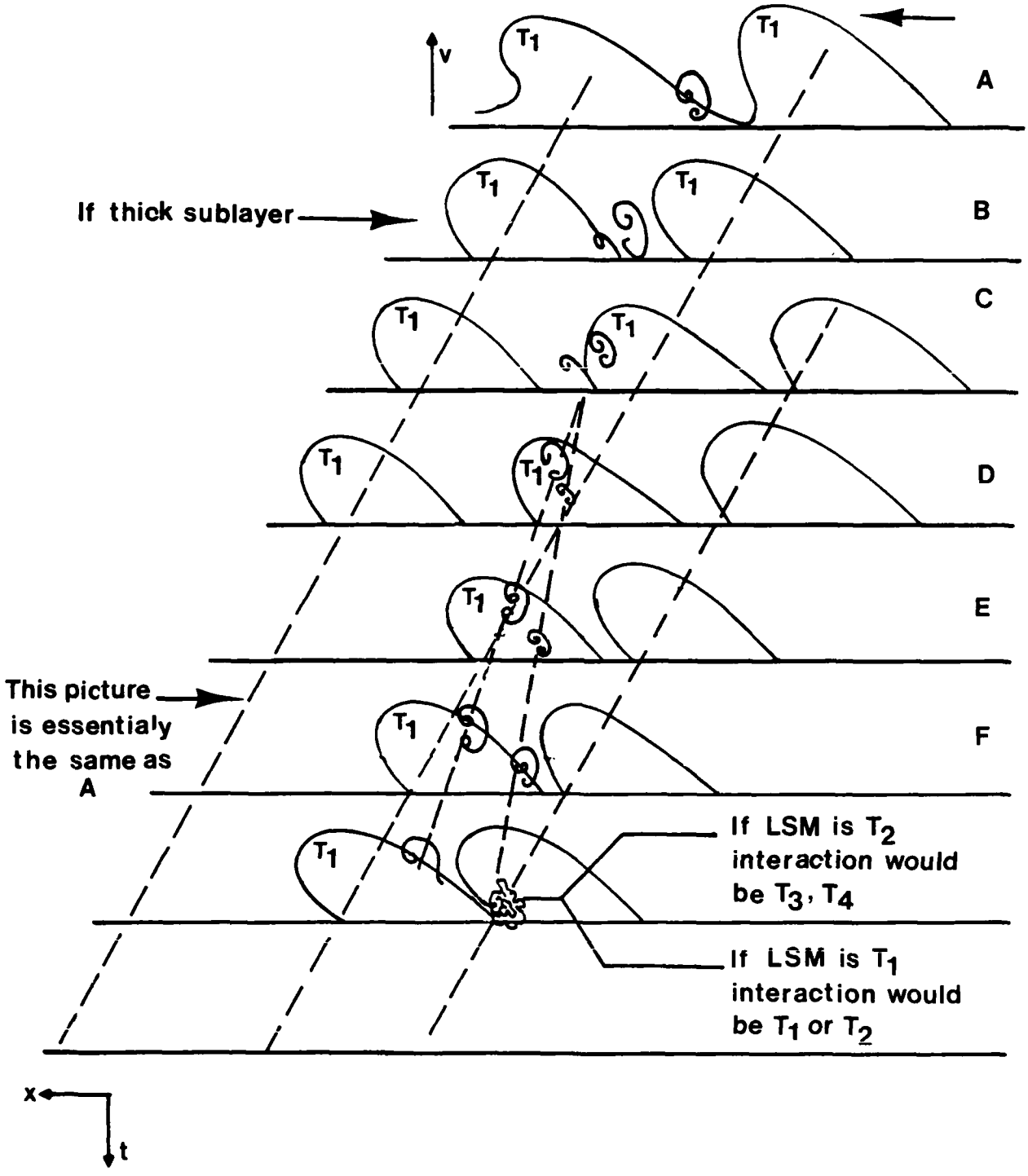

Fig. 29 Space-time picture showing the role the large scale motions play in the Typical eddy paths. When a large scale motion of Class A (labeled Tl in the figure) is followed by another large scale motion of Class A, and the sublayer is thick, the Typical eddy will result in a Type 2 interaction, which results in a hairpin that is induced by the Typical eddy to move out of the wall region and become another Typical eddy. Depending upon the Class of large scale motion that follows, the new Typical eddy can evolve in any of the ways discussed in the text.

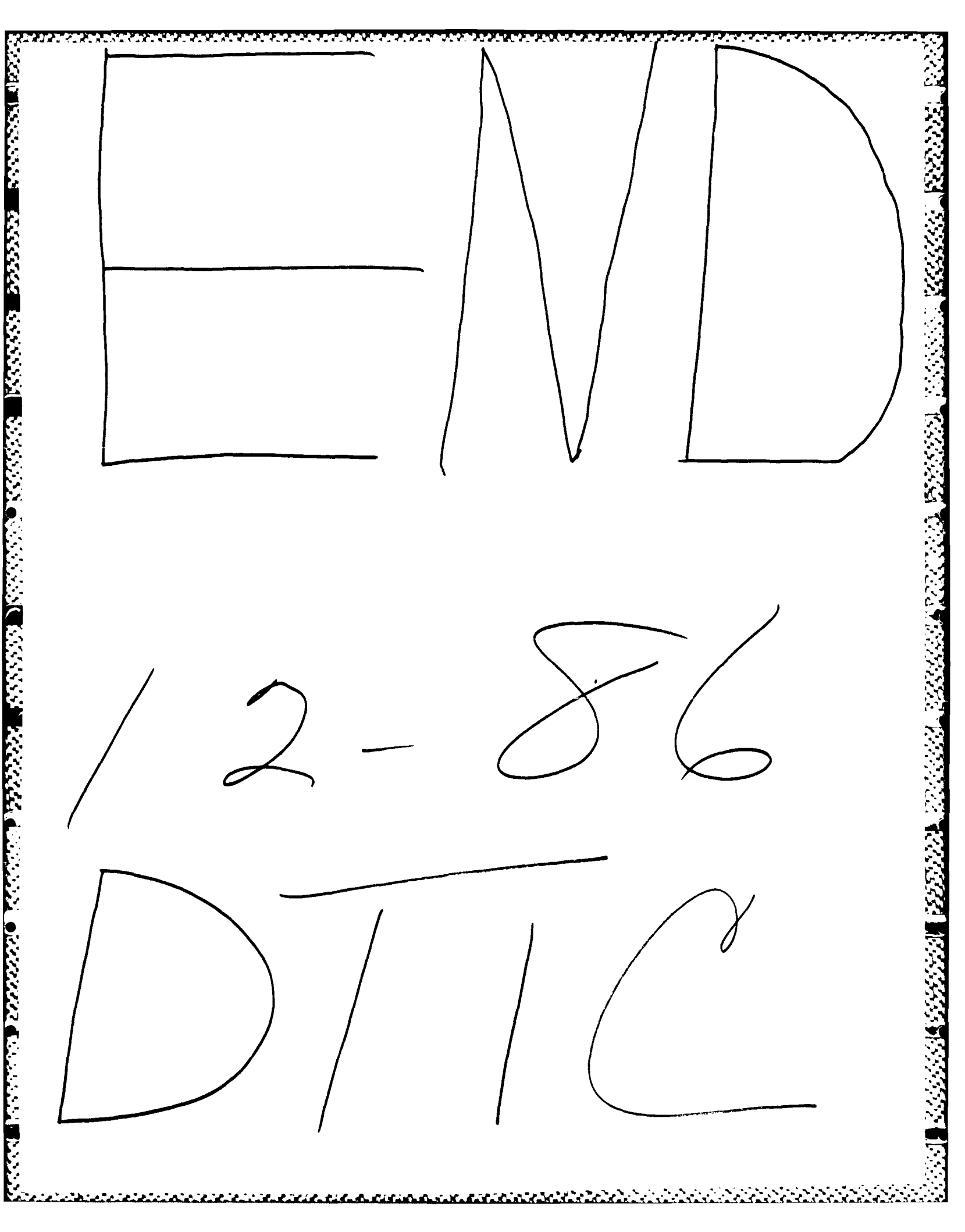
END
12-86
DTIC